

# Propagation and Optimisation

## Assignment III

Daniel Calliess, Mitchell van Doorn, Lorenz Veithen, Jesse Voskuilen

DELFT UNIVERSITY OF TECHNOLOGY  
FACULTY OF AEROSPACE ENGINEERING  
AE4866-1  
PROPAGATION AND OPTIMISATION IN ASTRODYNAMICS

---

## Lunar Ascent Trajectory Propagation and Optimisation

Design Space Exploration and Optimisation Problem Formulation

---

Lecturers: Dr. D. Dirkx

Github repository link: [https://github.com/LorenzVeithen/Propagation\\_Optimisation\\_Group\\_2D\\_2023](https://github.com/LorenzVeithen/Propagation_Optimisation_Group_2D_2023)

June 15, 2023

Name	Student Number	Hours Spent
Daniel Calliess	4869710	$\approx 56h$
Mitchell van Doorn	4954297	$\approx 45h$
Lorenz Veithen	5075211	$\approx 40h$
Jesse Voskuilen	4795768	$\approx 50h$

Cooperating Groups:



<sup>1</sup>Cover Image URL: [https://commons.wikimedia.org/wiki/File:Artist\\_concept\\_of\\_lunar\\_module\\_lifting\\_off\\_from\\_the\\_surface\\_of\\_the\\_moon.jpg](https://commons.wikimedia.org/wiki/File:Artist_concept_of_lunar_module_lifting_off_from_the_surface_of_the_moon.jpg)

## 1 Model Selection

In this section, the results from the previous (individual) analysis are discussed, and a consensus is reached on the model settings and optimisation formulation.

### 1.1 Problem Definition

Considering the model numerical and physical accuracy requirements, all team members kept the preliminary values given in the original project description. Following, based on the work provided in [1], requirements on the velocity and mass state variables' accuracy were added, due to their mission criticality. The ascent aims to reach the initial position of the rendezvous approach, for which initial relative distances and velocities of the order of 1 km and 10 m/s respectively are common [2], and an error of  $\approx 1\%$  is deemed permitted<sup>1</sup>. A physical error of only 0.01 kg for the propellant mass ( $\approx 0.0004\%$  of total), due to its mission criticality and to ensure compliance with the velocity accuracy (0.01 kg of propellant difference can lead to a change in  $\Delta V$  of 0.01 m/s, which is smaller than PROP-2). Furthermore, all members required the numerical error to be two orders of magnitude lower than the physical error, and the benchmark error three orders of magnitude lower than the numerical one. This permits to guarantee that the deviations obtained during the mission will only result from inaccuracies in the physical model itself, rather than arising from the propagation. Finally, PROP-4 was reduced<sup>2</sup> from 2 s to 1 s to ensure that two times more runs can be performed during the optimisation process<sup>3</sup>, which significantly increases the probability of finding the global optimum.

Table 1: Propagation requirements.

REQ ID	Requirement
PROP-1	The position accuracy of the physical modeling shall be 10m or smaller.
PROP-1.1	The numerical position accuracy shall be 0.1m or smaller.
PROP-1.2	The benchmark position accuracy shall be 1e-4m or smaller.
PROP-2	The velocity accuracy of the physical modeling shall be 0.1m/s or smaller.
PROP-2.1	The numerical velocity accuracy shall be 1e-3m/s or smaller.
PROP-2.2	The benchmark velocity accuracy shall be 1e-6m/s or smaller.
PROP-3	The physical mass modeling accuracy shall be 0.01kg or smaller.
PROP-3.1	The numerical mass accuracy shall be 1e-4kg or smaller.
PROP-3.2	The numerical mass accuracy shall be 1e-7kg or smaller.
PROP-4	CPU time per run shall be 0.5s or smaller.

Table 2: Propagation settings based on previous individual work of the team members. PM=point-mass gravity field, SH=spherical harmonics gravity field, ToL= (relative and absolute) tolerance.

Setting	Calliess [3]	Doorn [4]	Veithen [1]	Voskuilen [5]
Integrator	RKF4(5) ToL=1e-8	RKF7(8) ToL=1e-9	RKF4(5) ToL=1e-8	RKF7(8) ToL=1e-9
Propagator	Cowell	Cowell	Cowell	Cowell
Acceleration	Thrust, Earth PM, Moon SH (128,128)	Thrust, Earth PM, Moon SH (124, 124)	Thrust, Earth PM, Moon SH (75, 75)	Thrust, all planets & sun PM, Moon SH (64,64)
Model	Keplerian ephemeris, Spice Moon rotation Oblate spheroid	Constant ephemeris, Spice Moon rotation, Spherical shape	Constant ephemeris, Spice Moon rotation, Spherical shape	Spice ephemeris, Spice Moon rotation, Spherical shape

In order to fit the numerical accuracy requirements, while ensuring robustness with respect to the thrust input parameters to be optimised for, each member selected a combination of integrator-propagator settings. The entire team selected a Cowell propagator in their individual work, with the main reason being that it provides very similar performance to an Encke propagator (if not better), while being more robust (with respect to the thrust parameters) due to its simple formulation. Additionally, the Encke formulation was designed for lightly perturbed orbits, meaning that it loses most of its advantages in the present case (thrust is a large perturbation). Furthermore, all other propagators failed to propagate until the end of the trajectory in [1, 3, 4], and did not show any significant advantage in [5]. Following, it is seen from Tab. 2 that Calliess [3] and Veithen [1] selected RKF4(5), while Doorn [4] and Voskuilen [5] opted for RKF7(8), as integrator (with a Cowell propagator). While in the former cases, RKF4(5) came out as a clear best choice (and RKF7(8) had average performance), it was still a very good option in [4]. Voskuilen [5] did not select RKF4(5) for further

<sup>1</sup>Could be corrected through the use of a Guidance, Navigation, and Control System.

<sup>2</sup>Based on the results of each member's integrator-propagator selection.

<sup>3</sup>Was 0.5s in [1] but consideration of a wider range of propagations on the different computers showed that this requirement was too strong.

analysis despite similar performances to the RKF7(8) integrator in preliminary assessments, but neglecting the option this early in the process is considered as a mistake. While the input parameters considered in previous analyses only give a small sample size of the design space, the RKF4(5) integrator proved itself to be robust and yielded consistently good performance (where RKF7(8) was significantly worse in [1, 3]), and was therefore chosen for the subsequent work. The tolerance to be selected will be considered in Subsection 1.3.

Following, each member selected acceleration and model environments, with the results shown in Tab. 2. All came to the conclusion that the engine thrust, Earth PM, and Moon SH form the most significant parts of the acceleration environment (changes the trajectory by more than 10% of the physical requirements). However, Voskuilen [6] determined that the third body accelerations of the other planets and the Sun are necessary to meet PROP-1. This was determined to be a mistake by running his numbers in Veithen [7]'s program, showing that the same conclusions (as other members) should have been drawn. The main remaining point of difference is then the Degree and Order (D/O) of spherical harmonics to be included. For the purpose of this work, D/O up to (100, 100) were selected, resulting in a maximum position error of the order of 5 m [6, 7], and a computation time 18.9% larger than the Moon PM. This choice (which violates the 10% guideline) is a result of the trade-off between accuracy and computational efficiency for the SH selection, as PROP-1,2 and PROP-4 cannot all be satisfied at the same time [7].

Considering the environment models, [8, 9, 7] came to the conclusion that the ephemeris model could be simplified while ensuring that the PROP-1,2,(3) are satisfied. However, Calliess [8] did not consider the constant ephemeris model, which was found to be sufficient by the other two. The short mission time (1.9e-2% of the Moon's orbital period) permits to fix the position of the Earth and Moon in the Cartesian space to simplify the propagation. On the other hand, Voskuilen [6] selected the full spice ephemeris model to ensure a maximum accuracy while satisfying the 2 s CPU time requirement. This was determined to be a mistake in the context of an optimisation problem: the present work aims to prepare a propagation setup for an optimisation procedure, where it is especially important to run numerous propagations to find the global optimum. For this reason, a model which is known to be less accurate, but permits to run many more propagations is desired<sup>4</sup>. Furthermore, all members determined that the most accurate rotation model available in TUDAT should be used for the Moon. This is a result of the spherical harmonics of the Moon being a major disturbance (compared to Moon PM) in the propagation, and being dependent on the body orientation. At last, all members determined that the shape model had no influence on the trajectory, and most decided to use the spherical model for simplicity. However, the oblate spheroid shape model does not increase the computational time (only used to compute dependent variables), and permits to stay closer to the real physics of the problem<sup>5</sup>. In the following, a constant ephemeris, Spice rotation, and oblate spheroid shape model will be used.

Table 3: Selected propagation settings.

Integrator	Propagator	Accelerations	Environments
RKF4(5)	Cowell	Thrust, Earth PM, Moon SH (100, 100)	constant ephemeris, Spice Moon rotation, Oblate spheroid

## 1.2 Preliminary Optimisation Problem Formulation

In this section the results from the previous individual assignments is taken as starting point to define objective and constraints function and a suitable decision variable space for optimisation.

### 1.2.1 Objective Functions

#### Minimise propellant mass

Veithen [7], Doorn [9] and Calliess [8] chose to minimise consumed propellant mass, while Voskuilen [6] selected accuracy and runtime as objective functions. It was chosen to minimise the consumed propellant mass  $M_f$  during the lunar ascent trajectory, due to its importance as performance parameter in space missions. For a space mission fuel mass is a key criteria as it is very costly to launch mass to space, especially all the way to the lunar surface. Every kg of fuel saved would give room for valuable science equipment, resources or a decreased total mass and thus cost. This first objective is calculated from the difference in initial and final mass leading to Eq. (1), with  $t_0$  and  $t_e$  the initial and final propagation time. The mass is a propagated state and will be directly obtained from the state vector.

$$M_f = M(t_0) - M(t_e), \quad \text{Objective1 : } \min(M_f) \quad (1)$$

#### Minimise $\Delta V_{tar}$ required to reach target orbit

A second objective that directly competes with objective 1 was not trivial to find and all team members had different approaches to this. Voskuilen [6] chose accuracy and run time as objective which were found not to be relevant objective functions but rather requirements while Veithen [7] did not define a second objective function next to minimising fuel

<sup>4</sup>A higher fidelity simulation of the optimum value found can always be considered to verify the results

<sup>5</sup>But requires modifying the initial state to 100m above the real surface.

mass. Calliess [8] proposed to minimise the relative velocity difference to a target spacecraft and Doorn [9] proposed to minimise corrective delta-V needed after docking to the lunar command module. The team decided that the aim is to optimize an ascent trajectory to reach a specified target orbit and dock a potential second spacecraft waiting there. The target orbit is assumed to be a 100 km altitude (with respect to the launch site) circular orbit with an inclination of 2.2°. The inclination was chosen as most individual trajectories from previous work resulted in that inclination. Furthermore, once the optimised trajectory has been determined, it can be ensured that the two spacecrafts meet by launching the lunar module when the command module position in the orbit is adequate.

Therefore, the second objective is to minimize the  $\Delta V_{tar}$  required to reach the specified target orbit, once the lunar module reaches 100 km altitude. This objective is directly competing with objective 1 since both are minimising the usage of propellant mass. There is a clear trade-off between spending more fuel to get closer to the target orbit but having less fuel to correct later or vice versa. Each trajectory is terminated at 100 km by performing a line search, to ensure a fair comparison between the different trajectories<sup>6</sup>. Upon termination, two manoeuvres are performed: circularisation of the orbit ( $\Delta V_1$ ) and an inclination change ( $\Delta V_2$ ). The difference in propagated and target velocity vector can be described with spherical velocity coordinates. According to (Mooij, 1994), the flight path angle ( $\gamma$ ) is the angle between velocity vector ( $\vec{V}$ ) and local horizontal [10]. The cosine rule is applied to find the  $\Delta V$  required to change velocity assuming an impulsive shot and combined change in velocity magnitude and  $\gamma$ , leading to manoeuvre 1 in Eq.(2):

$$\Delta V_1 = \sqrt{V_f^2 + V_c^2 - 2V_f V_c \cos(\gamma)} \quad (2)$$

where  $V_f$  is the final velocity obtained from the propagated state vector and  $V_c$  is the circular target velocity. The inclination change is assumed to be executed at either the ascending or descending node and is found with Eq. (3) [2]:

$$\Delta V_2 = 2V_c \sin(\Delta i/2) \quad (3)$$

where  $\Delta i$  is the change in inclination. Combining the two manoeuvres leads to the second objective function, shown in Eq. (4). Adjustments in the Right Ascension of the Ascending (RAAN) node were not considered as those manoeuvres are generally inexpensive and only the relatively small perturbations in RAAN are expected.

$$Objective2 : \min(\Delta V_{tar}), \quad \Delta V_{tar} = \Delta V_1 + \Delta V_2 \quad (4)$$

### 1.2.2 Constraint Functions

Constraints for the optimisation process are selected to define infeasible trajectories. The launch location and thus initial state is fixed by defining the initial spherical coordinates: radius ( $r_0$ ), latitude ( $\phi_0$ ) and longitude ( $\lambda_0$ ). Additionally, initial velocity ( $v_0$ ), heading angle ( $\psi_0$ ), and flight path angle ( $\gamma_0$ ) are defined. The minimum altitude is set to 0 m to terminate the propagation once the spacecraft impacts the ground. The maximum time ( $t_{max}$ ) that the propagation can run is equal to one hour (or  $t_{max} = 3,600$  s). This is to prevent unnecessary computations for clearly inefficient or malfunctioning trajectories. The time is taken directly from the state vector. The specific impulse was increased from 311 s to 452 s taken from Space Shuttle [11], as that is more realistic of current rocket engine performances and allowed for a more realistic design space.

Table 4: Constraint functions used for optimisation with preliminary values for constraint boundaries.

Constraint	Description
$r_0 = r_M + h_0, \quad \lambda_0 = 23.4333^\circ, \quad \phi_0 = 0.6875^\circ$	Initial state
$\gamma_0 = 89^\circ, \quad v_0 = 10m/s, \quad \psi_0 = 90^\circ$	Initial state
$h_{min} > 0km$	Minimum altitude
$t_{max} \leq 3,600s$	Maximum time
$I_{sp} = 452s$	Specific impulse
$M(t_e) > M_{dry} = 2250kg$	Minimum mass
$a_{max} < 6g$	Maximum mechanical load
$\psi_0 = \frac{T}{M_0 g_m} > 1$	Minimum initial thrust load
$\dot{\theta}_{max} < 20deg/s$	Thrust angle rate constraint
$\Delta V_{buffer} = I_{sp} g_0 \ln\left(\frac{M(t_0)}{M(t_e)}\right) - \Delta V_{tar} \geq 0m/s$	Check if target orbit is reachable with remaining fuel mass

The initial thrust load ( $\psi_0 > 1$ ) constraint ensures lift off, and is computed from the thrust magnitude  $T$ , the Moon gravitational acceleration  $g_m$  and vehicle initial mass  $M_0$ . A maximum mechanical load is set to 6 Earth g's to avoid any failure of the payload or the humans on-board. Preliminary analysis of the individual assignments showed some strange features due to rapid nodal changes. Sometimes the thrust angle would change over 40 degrees in several seconds, which

<sup>6</sup>For trajectories stopping below 100 km, an additional Hohmann transer

is somewhat unrealistic. To handle this a constraint is set on the maximum thrust angular rate  $\dot{\theta}_{max}$ . This rate is calculated by retrieving the thrust angle per time step and then calculating the time derivative of it with a forward finite difference scheme. Maximum thrust angle rates of rocket engines vary a lot, but rates up to 20 deg/s are possible (Sutton [11], table 16.2). The propagation is terminated once all fuel has been used, this is when the minimum mass is reached. In this case the final mass  $M(t_e)$  is equal to the dry mass  $M_{dry} = 2250$  kg. The last constraint function is an important connection between both objectives and makes sure the proposed trajectory is physically possible: once the lunar ascent trajectory is done and consumed fuel mass is known, it will be verified whether the remaining propellant is sufficient to perform the proposed manoeuvre of objective 2 and reach the target orbit. Any trajectory where the fuel mass remaining after engine cut-off is less than the fuel mass needed for the corrective manoeuvre is not feasible. The remaining 'allowed'  $\Delta V$  after engine cut-off is found from the rocket equation and the final and initial mass from the state vector. The  $\Delta V_{buffer}$  is defined as difference in allowed  $\Delta V$  and objective 2 (already quantified as  $\Delta V$ ) and must be positive.

### 1.2.3 Decision Variables

Voskuilen [6], Doorn [9] and Calliess [8] decided to use the provided thrust parameters as decision variables while Veithen [7] proposed to also vary the thrust magnitude at each node. The team members agreed that this extension, although more realistic, would make the design space too large to analyse given the limited time for this assignment, therefore, the standard seven thrust parameters are chosen as decision variables. Provided that more time is available both time variable thrust and a three-dimensional parameterisation of the thrust vector would be possible additions to the current model, making the trajectory more realistic and possibly finding a better optimum.

Table 5: Decision variables and boundaries of decision variable space.

Decision variable	Definition and boundaries
Thrust magnitude	$5kN \leq T \leq 20kN$
Node spacing	$10s \leq \Delta t \leq 100s$
Thrust angle at node 1	$-0.1rad \leq \theta_1 \leq 0.1rad$
Thrust angle at node 2	$-0.5rad \leq \theta_2 \leq 0.5rad$
Thrust angle at node 3	$-0.7rad \leq \theta_3 \leq 0.7rad$
Thrust angle at node 4	$-1.0rad \leq \theta_4 \leq 1.0rad$
Thrust angle at node 5	$-1.6rad \leq \theta_5 \leq 1.6rad$

#### Thrust magnitude

Varying the thrust setting ( $T$ ) allows for more efficient flight paths, which in turn can optimize fuel usage. The minimum and maximum thrust magnitude is set between 5 and 20 kN as the nominal thrust of the lunar module during Apollo 11 was 15.5 kN [12] and this is a realistic obtainable thrust range around that value.

#### Node spacing

The node spacing ( $\Delta t$ ) determines the spacing in time between the five nodal points where the thrust angle and magnitude is defined. Changing this spacing would allow for more rapid changes early in the trajectory or more spread out dynamical changes during the ascent in search of an optimal flight path. The maximum node spacing of 100 s is chosen to ensure that all thrust angle nodes lie inside the typical propagation time of around 450s. Larger node spacing values might push the final thrust angle outside the ascent trajectory. A minimum node spacing of 10 s prevents too rapid thrust angle rotation rates and ensures a smooth trajectory. Previous assignments showed that too low node spacing values result in unrealistic and sometimes erratic behaving trajectories.

#### Thrust angles

Defining the thrust angles at the nodes ( $\theta$  in rad) results in a certain flight path. Varying this would give rise to different ascent profile shapes in search of the best one. The provided thrust angle boundaries are taken as starting point and adapted. The first node is constraint to mostly vertical thrust ( $\pm 0.1rad$ ) which is typical for most rocket ascent trajectories and prevents too much horizontal motion that could lead to terrain impact, while subsequent nodes allow more freedom in thrust angles. This follows from the large variety in possible trajectories to reach a circular orbit and that rockets will usually follow a gravity ascent type trajectory which is within this allowed ascent boundaries. The final node angle boundaries are increased beyond 90 degrees to ( $\pm 1.6rad$ ), as it is expected that the lunar module might need to burn horizontally to reach its target orbit effectively.

### 1.3 Verification of Numerical Accuracy and Objective and Constraint values

Compliance to PROP-1.1, -2.1 and -3.1 was verified by repeating the numerical accuracy analysis performed in [1, 3, 4, 5]. First, a benchmark was generated (with the selected settings) for each propagation using a RKF7(8) integrator, with a fixed step size of  $\Delta = 0.1s$ : it is clear from Fig. 1 that this benchmark fits PROP-1.2 (for all trajectories) and is in the Local Truncation Error (LTE) region. Note that the velocity and mass accuracies were found to be less constraining for each propagation, and only the benchmark position accuracy was considered. Based on those benchmarks, the numerical accuracy of the model defined by the settings in Tab. 3 was verified, as shown in Figs. 2 and 3, showing that PROP-1

and PROP-2 are met for all trajectories<sup>7</sup> using a tolerance of 1e-8. The tolerance of 1e-7 suggested by [1] was found to be insufficient for other trajectories ([3]). Although the input parameters considered are only a very small sample of the feasible design space, it will be assumed throughout the rest of this work that the combination of Cowell and RKF4(5) with ToL=1e-8 (absolute and relative), yields propagations which consistently satisfy PROP-1.1, -2.1, and -3.1. Furthermore, it was found that the run time for each propagation is about 0.4s (across all team members' computers), thereby meeting the PROP-4 requirement.

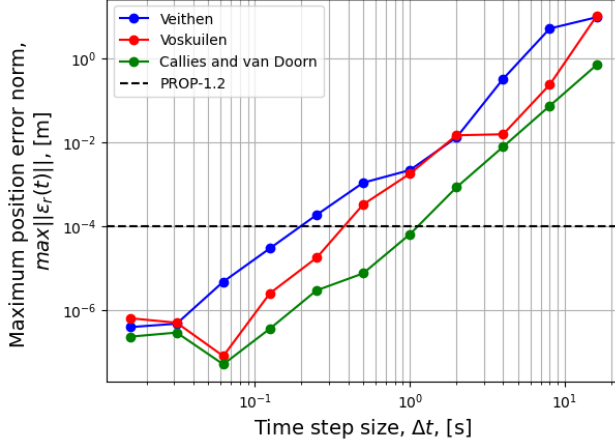


Figure 1: Benchmark position accuracy as a function of the time step size.

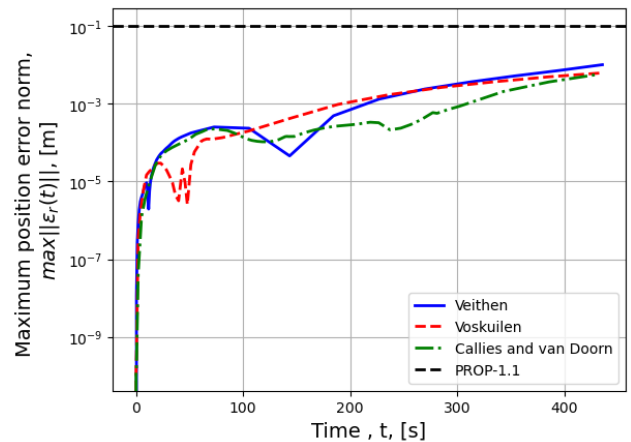


Figure 2: Position accuracy as a function of time for each trajectory, with a tolerance (absolute and relative) of 1e-8.

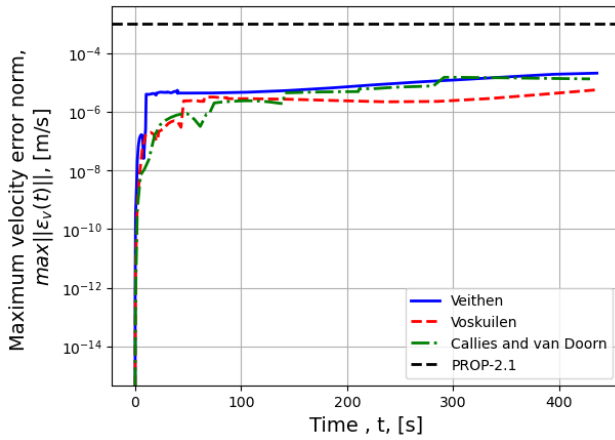


Figure 3: Position accuracy as a function of time for each trajectory, with a tolerance (absolute and relative) of 1e-8.

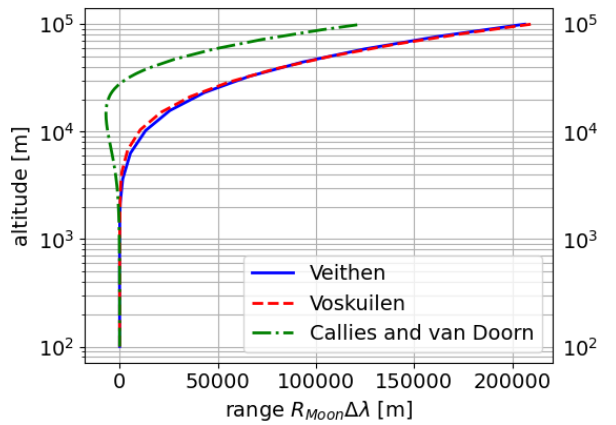


Figure 4: Range vs altitude for all four individual settings from [7, 8, 9, 6].

In Tab. 14, values for the objective and (relevant) constraint functions are calculated. Also, in Fig. 4, the altitude is plotted against the range (which is computed with  $R_{Moon}\Delta\lambda$ , where  $\lambda$  is the longitude) for all 4 individual settings in order to visualize how the trajectories differ from one another.

Table 6: Objective and (relevant) constraint values for each individual settings.

Settings (student number)	Doorn [4]	Veithen [1]	Voskuilen [5]	Calliess [3]
<b>Objective values</b>				
$\Delta V_{tar}$ needed [m/s]	1536	1411	1499	1536
Propellant mass used [kg]	1943	2011	1941	1943
<b>Constraint values</b>				
Maximum altitude [m]	100000	100000	100000	100000
Maximum time [s]	489	437	566	489
Maximum mechanical load / acceleration [ $m/s^2$ ]	3.60	4.38	2.84	3.60
Minimum initial thrust load [-]	1.59	1.84	1.37	1.50
Maximum thrust angle rotational rate [deg/s]	1.10	12.05	2.25	1.10
$\Delta V_{buffer}$ [m/s]	-916	-868	-877	-916

<sup>7</sup>The mass accuracy was always on the other of rounding errors, as it is a simple linear model for constant thrust application.

As can be seen in Tab. 14, all settings have negative  $\Delta V_{buffer}$  values, meaning once the final altitude of 100 km is reached there is not enough fuel left to reach the target orbit. Therefore, per definition all settings provide infeasible solutions. Other constraints are not violated, and objective values are similar.

## 2 Design Space Exploration

### 2.1 Sobol Distribution

For both MC analysis, a sobol distribution was used to generate the decision variables, because a sobol distribution fills the range of decision variables more densely when compared to a standard random generator. It was made sure that the order in which a consecutive run chooses one of these generated values was randomized (since the sobol distribution generates a list in a sequence which is always the same). In Tab. 7, the maximum difference between 2 consecutive values of each decision variable is listed, if the values were to be put in a list, sorted by increasing magnitudes. As can be seen the sobol distribution gives a denser output compared to the uniform distribution.

Table 7: Sobol distribution for decision variables (4096 runs)

Decision variable	Definition and boundaries	Maximum difference between two consecutive values - sobol	Maximum difference between two consecutive values - uniform
Thrust magnitude	$5kN \leq T \leq 20kN$	7.324 e-03 [kN]	3.364 e-02 [kN]
Node spacing	$10s \leq \Delta t \leq 100s$	4.394 e-02 [s]	2.445 e-2 [s]
Thrust angle at node 1	$-0.1rad \leq \theta_1 \leq 0.1rad$	9.765 e-05 [rad]	4.283 e-04 [rad]
Thrust angle at node 2	$-0.5rad \leq \theta_2 \leq 0.5rad$	4.883 e-04 [rad]	2.256 e-03 [rad]
Thrust angle at node 3	$-0.7rad \leq \theta_3 \leq 0.7rad$	6.835 e-04 [rad]	2.497 e-03 [rad]
Thrust angle at node 4	$-1.0rad \leq \theta_4 \leq 1.0rad$	9.765 e-04 [rad]	4.734 e-03 [rad]
Thrust angle at node 5	$-1.6rad \leq \theta_5 \leq 1.6rad$	1.562 e-04 [rad]	7.278 e-03 [rad]

### 2.2 One at a Time Monte-Carlo

A one-at-a-time Monte-Carlo analysis is performed varying each decision variable independently while keeping the rest equal to the nominal parameters. The Sobol distribution is used replacing the default pseudo-random distribution, see Subsection 2.1, to ensure a more structured input parameter density. The nominal parameters used for this simulation are obtained from Veithen [7] and are: [10000.0, 80.0, 0.05, 0.25, 0.35, 0.5, 0.65]. 400 runs are performed per parameter, hence a total of 2800 simulations were run. The influence of each parameter will be analysed against both objectives and the three selected relevant constraints. Looking at Tab. 4, most constraints are by default satisfied (eg.  $t_{max}$ ), fixed in the simulation (eg.  $I_{sp}$ ) or decision variable boundaries (eg. thrust angles) while only some provide additional inside into the problem and are thus 'relevant'. These are the maximum acceleration (g-load), maximum thrust angle rate (deg/s) and the  $\Delta V_{buffer}$  (m/s). To show that the number of runs per parameter is sufficient, a pilot run with 200 runs is performed and the variation of the mean value of the two objectives and three relevant constraints is recorded when changing to 400 runs. Tab. 8 shows that the mean of these parameters changes at most by 2.75% (for  $\Delta V_{buffer}$ ) which is small enough to draw preliminary conclusions on the design space and decision variable correlations.

Table 8: Variation in mean of objective and relevant constraint functions using Monte-Carlo simulation with 200 and 400 runs.

Name of response variable	Objective 1	Objective 2	$a_{max}$	$\dot{\theta}_{max}$	$\Delta V_{buffer}$
Variation of mean of selected response variable: 400 wrt 200 runs per parameter	-0.38 %	1.50 %	-1.06 %	-0.90 %	-2.75 %

The objective space in Fig. 5 shows that thrust magnitude and last thrust angle  $\theta_5$  are the most influential parameters on both objectives. Only the runs not violating any constraints are shown, resulting in fuel mass consumption ranging between 1200 to 2000 kg and corrective  $\Delta V$  needed between 200 to 1600 m/s. The fuel mass consumed goes above 4 tons and corrective  $\Delta V$  needed above 2 km/s including non-feasible runs. The other decision variables have minor effect on both objectives. This relates to the lunar ascent as expected since thrust magnitude directly relates to mass flow and fuel consumption and the last thrust node defines the burn direction for most of the trajectory and is thus most influential. Since the propagation time is 450 s and most node spacings are between 10 s and 100 s, most of the trajectory time is spent with the last thrust angle setting. Fig. 6 shows that increasing node-spacing minimises objective 1 but maximises objective 2 and vice versa, hence the objectives are directly computing. No constraints are violated for this decision variable with their limiting values at  $a_{max} = 0.22g$ ,  $\dot{\theta}_{max} = 1.5deg/s$  and minimum  $\Delta V_{buffer} = 764.84$ . Too low thrust magnitude leads to the lunar module impacting the surface, see Figs. 7 and 8. It is large enough to lift off ( $\psi_0 > 1$ ) but the spacecraft turns and there is not enough thrust to counter gravity anymore for these trajectories. Maximum acceleration constraint

is most influenced by thrust magnitude reaching values of 0.45 g at highest thrust values, this is expected since vehicle thrust directly defines the acceleration settings.

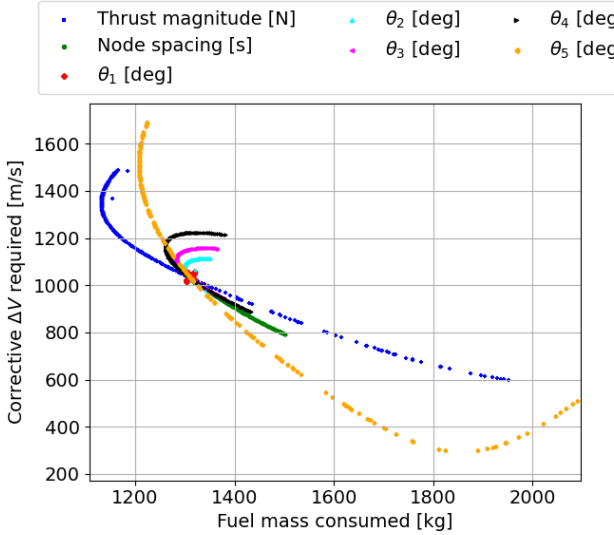


Figure 5: Objective space showing fuel mass consumed (kg) and corrective  $\Delta V$  required (m/s) for each parameter variation case.

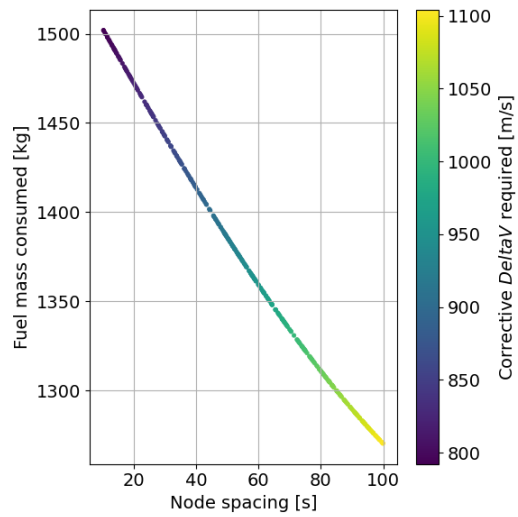


Figure 6: Fuel mass consumed (kg) and corrective  $\Delta V$  required (m/s) for variation in node spacing (s), showing that objectives are directly competing.

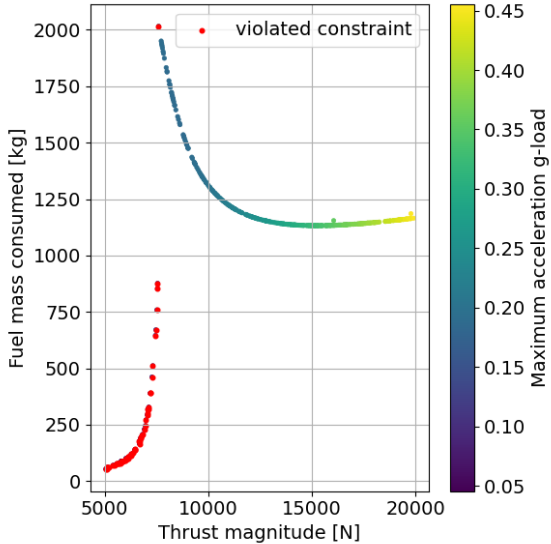


Figure 7: Fuel mass consumed (kg) and maximum acceleration ( $a_{max} < 6g$ ) for variation in thrust magnitude (N).

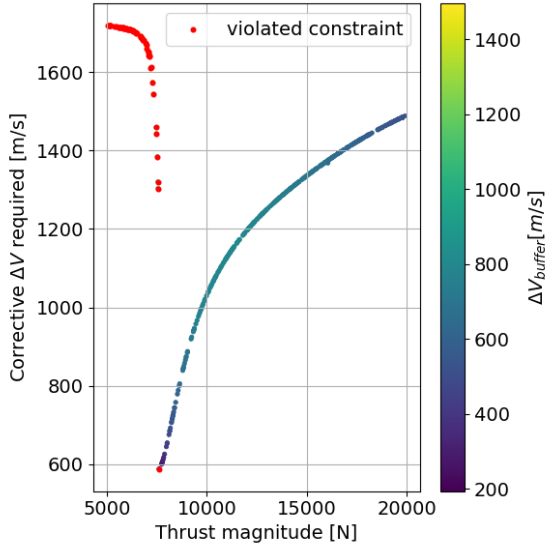


Figure 8: Corrective  $\Delta V$  required (m/s) and  $\Delta V_{buffer}$  (must be  $> 0$  m/s) for variation in thrust magnitude (N).

Figs. 9, 10 imply that each subsequent thrust angle is more influential on the objective. A low angle minimises objective 1 as that leads to a vertical trajectory and earlier termination conditions. Objective 2 is optimised with larger thrust angles, especially  $\theta_5$ . This is inline with theory as the target orbit velocity vector is at 90 deg flight path angle and the lunar module should ideally increase its flight path angle along the trajectory, to approach the target velocity vector and thus minimise objective 2. None of the constraint is violated or close to its limits for these 4 decision variables. Figs. 11 and 12 show that maximum angular rate is most influenced by  $\theta_5$  reaching around 1 deg/s. Most runs with negative  $\theta_5$  violate  $\Delta V_{buffer}$ , this constraint is most affected by this decision variable. This is expected since the target orbit is defined in eastward direction (2.2 deg inclination) and thus any thrust in negative direction (west) is slowing the spacecraft down or if launching in that direction it is impossible to correct for this  $\Delta V_{buffer}$  later.

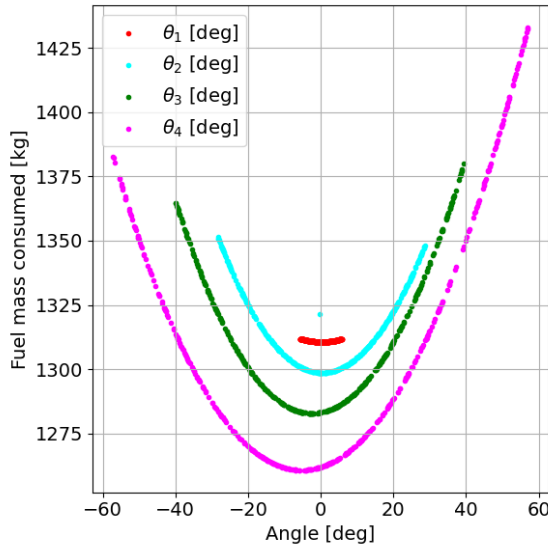


Figure 9: Fuel mass consumed (kg) for variation in  $\theta_1, \theta_2, \theta_3, \theta_4$  (deg). None of the runs violate any constraints.

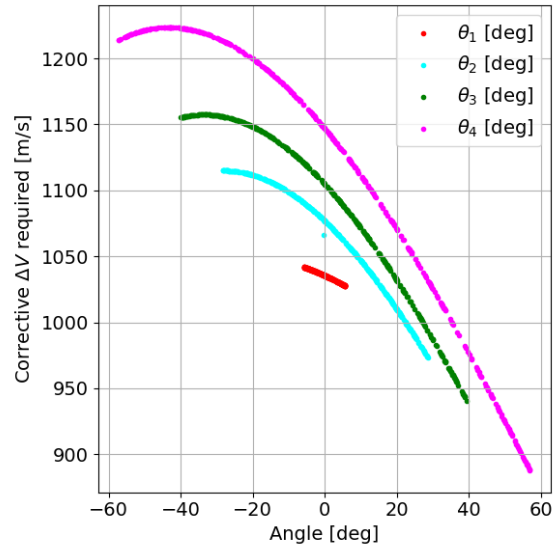


Figure 10: Corrective  $\Delta V$  required (m/s) for variation in  $\theta_1, \theta_2, \theta_3, \theta_4$  (deg). None of the runs violate any constraints.

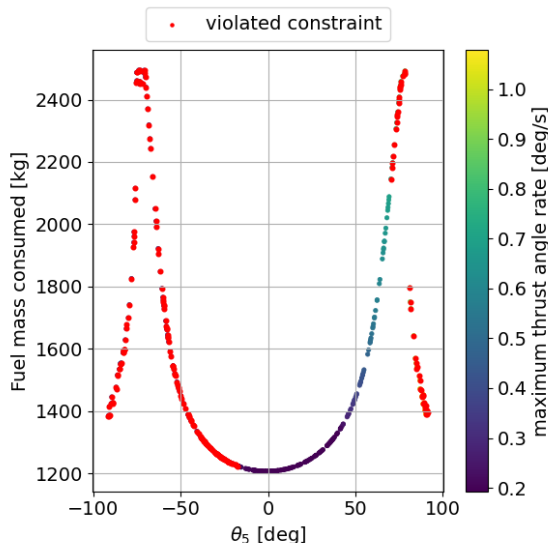


Figure 11: Fuel mass consumed (kg) and maximum thrust angle rate (must be  $< 20$  deg/s) for variation in  $\theta_5$  (deg).

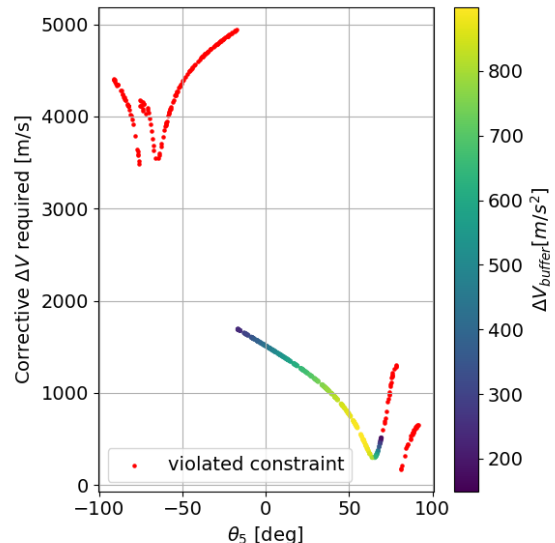


Figure 12: Corrective  $\Delta V$  required (m/s) and  $\Delta V_{\text{buffer}}$  (must be  $> 0$  m/s) for variation in  $\theta_5$  (deg).

### 2.3 Full Monte-Carlo

A full Monte Carlo analysis was done, where all decision variables were varied at the same time for each run of a trajectory. As stated in Subsection 2.1, a sobo distribution is used for generating the decision variables.  $2^{12}$ , or 4096, runs were performed in total. In the following figures, plots are shown for each objective and constraint function as a function of a decision variable that has a **strong** influence on that particular objective or constraint function. These plots will be discussed in more detail in this section.

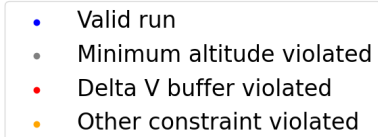


Figure 13: Legend applicable for all full MC plots

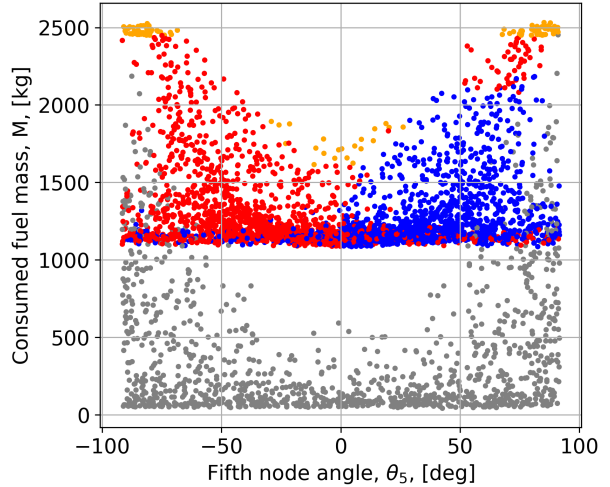


Figure 14: Consumed fuel mass as a function of fifth node angle.

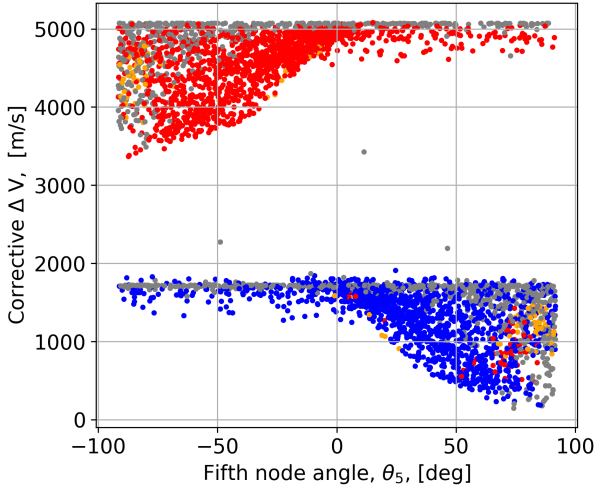


Figure 15: Corrective Delta V as a function of fifth node angle.

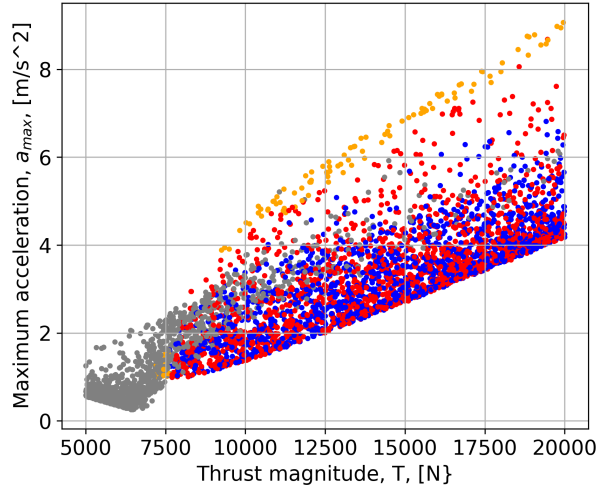


Figure 16: Maximum acceleration as a function of the Thrust magnitude.

For both objective functions the fifth node angle has shown to be the most influential decision variable, and objective functions as a function of it have been plotted in Figs. 14 and 15. Numerous simulations below the 1000 kg consumed fuel are crashes, caused either by small thrust magnitudes or trajectories that are too horizontal w.r.t. the moon's surface so that they don't ascent enough and get pulled back to the moon's surface again. Furthermore the plot shows that negative fifth node angles generally end up violating the Delta V buffer, which makes sense since then the thrust acts in opposite direction of the target orbit for the whole duration after node 5. This also explains the 'gap' in Fig. 15 as for negative fifth node angles the spacecraft diverges from its target orbit. Furthermore, the trend is that positive fifth node angles closer to 0 generally consume less fuel mass, but have a higher corrective Delta V. This makes sense as more vertical trajectories reach the target altitude of 100km faster (at which the simulation will stop) and more horizontal trajectories reach that altitude slower but once they do they are more aligned with the orbit direction. Fig. 16 shows the clear trend that for increasing the thrust magnitude, the maximum accelerations reached will generally be higher. Fig. 17 shows that smaller node spacing's have a higher change of resulting in higher maximum thrust angle rates. This makes sense: at every node the thrust angle is changed and the thrust angle per time step is calculated by a Hermite spline interpolation through these nodes. For a given set of node angles, the closer the nodes are together, the faster the rate of change of the thrust angle becomes. Furthermore, in Fig. 18 we again see that in general, for negative fifth node angles most runs violate the Delta V buffer, because their trajectory deviates from the target trajectory. Most trajectories that are valid have positive fifth node angles.

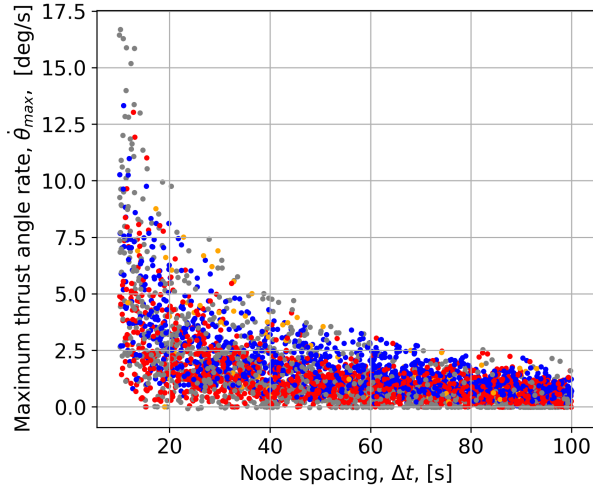


Figure 17: Maximum thrust angle rate as a function of the node spacing.

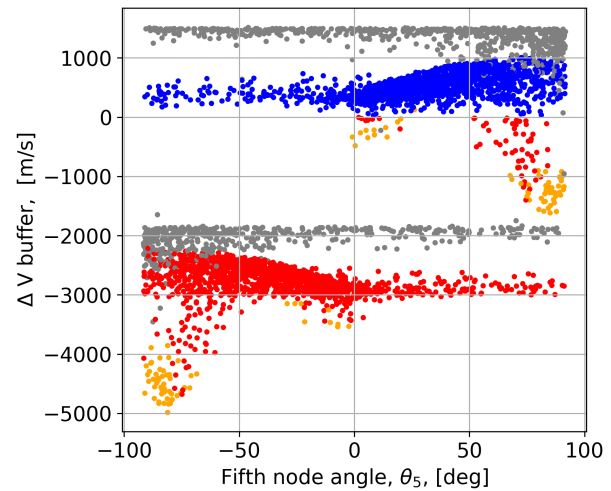


Figure 18: Delta V buffer as a function of the fifth node.

When the consumed fuel mass as a function of the fifth node angle is plotted with colorbars indicating the value of the Corrective delta V and the maximum acceleration (Figs. 19 and 20), some extra insights can be gained. Note that for these plots only the valid runs are plotted. In Fig. 19 it can be clearly seen that for lower consumed fuel mass, usually the corrective Delta V is larger and vice versa. Here and there, especially around the 1400kg consumed fuel mass and  $\theta_5 > 50\text{deg}$  region there are some data points (runs) though, that have a relatively low consumed fuel mass (of around 1400kg's thus) and also a relatively low Corrective delta V. These thus correspond to runs having a more efficient thrust profile. In Fig. 20 it can be seen how much Delta V buffer all valid runs have and it can be deducted that a lot of runs are also very close to the minimum Delta V buffer constraint of 0m/s, which is not ideal in terms of safety. In Figs. 21 and 22 the corrective Delta V is plotted against the fifth node angle with consumed fuel mass and Delta V buffer colorbars. For these plots the same insights can be gained.

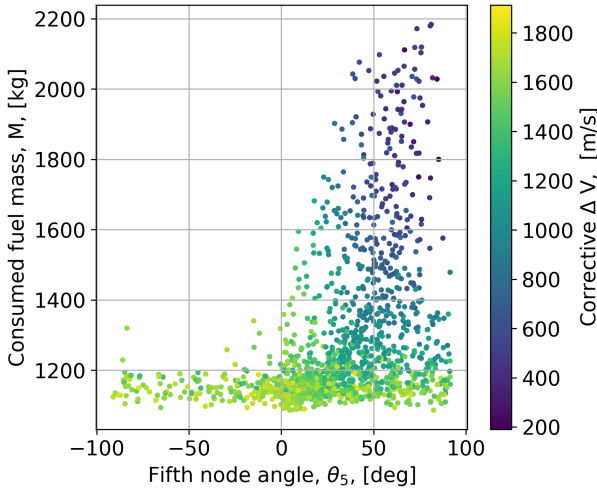


Figure 19: Consumed fuel mass as a function of fifth node angle with corrective Delta V colorbar.

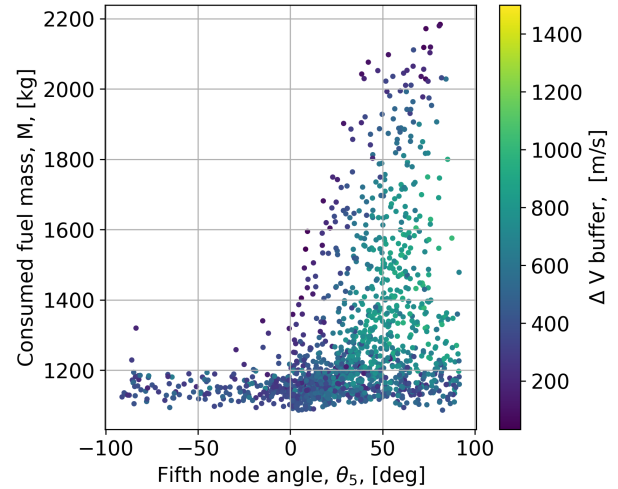


Figure 20: Consumed fuel mass as a function of fifth node angle with maximum acceleration colorbar.

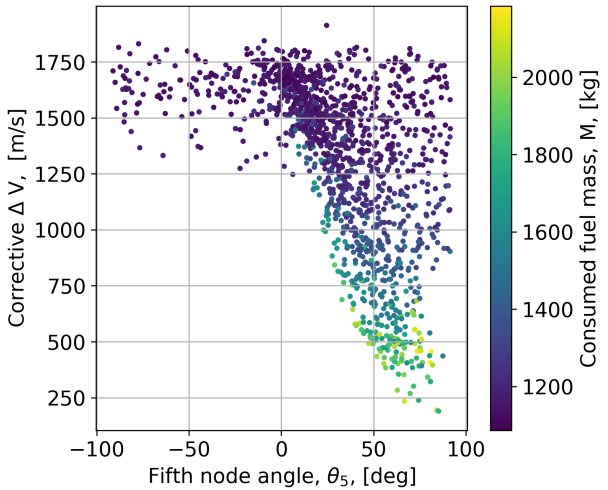


Figure 21: Corrective Delta V as a function of fifth node angle with consumed fuel mass colorbar.

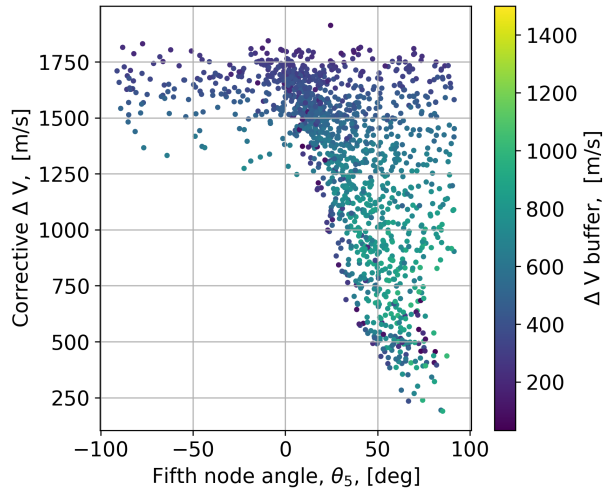


Figure 22: Corrective Delta V as a function of fifth node angle with maximum acceleration colorbar.

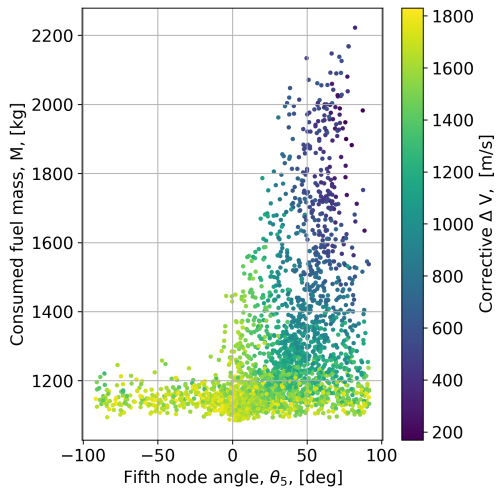


Figure 23: Consumed fuel mass as a function of fifth node angle with corrective Delta V colorbar for  $2^{13}$  runs.

For all the above plots in this section,  $2^{12}$  runs were done for the analysis. In order to show this amount in sufficient, and the conclusions and insights that are drawn are valid, an additional analysis was done with double the amount of runs, so  $2^{13}$  runs. As can be seen in Fig. 23, the results are similar when the consumed fuel mass is plotted against the fifth node angle with the corrective Delta V as a colorbar.

## 2.4 Monte Carlo Methods Comparison

A Monte-Carlo (MC) one-at-a-time simulation was performed in Subsection 2.2 and a full MC analysis in Subsection 2.3. From the one-at-a-time Monte-Carlo analysis it can be observed that thrust magnitude and the last thrust angle  $\theta_5$  are the driving decision variables, and the other decision variables show clear correlation to each objective and to some specific constraints. The full MC analysis showed a similar general trend for thrust and  $\theta_5$ , while for the other decision variables, no clear correlation to the values of the objectives and constraints could be deducted, (which is also why plots for those decision variables are not included in Subsection 2.3). The reason for the discrepancy in both models is that the one-at-a-time MC shows single independent effects of changing decision variables while the full MC shows varies all decision variables at the same time. It then makes sense that the trends in the driving decision variables remain visible in the full MC analysis while for decision variables having a smaller influence on the objective and constraint function values, it becomes harder to see correlations between them because the driving decision variables just influence the outcome too much. The thrust magnitude does only violate minimum altitude when varied independently but can violate all constraints when additional decision variables are varied at the same time, thus implying heavy interactions with those other decision variables, which is expected for full MC. The one-at-a-time MC shows that node spacing does not have big influence on the maximum thrust angle rate constraint but full MC shows much stronger effect on that constraint, going up to 16 deg/s. This is because when varying multiple subsequent angles instead of a single independent one, larger changes are possible if consecutive angles are a lot different from each other. Also, the maximum acceleration constraint ( $6 \text{ m/s}^2$ ) is not

violated for any run in the one at a time MC (Fig. 7), while for the full MC this happens and the maximum accelerations reached can be twice as much (Fig. 16). This is due to the fact that when varying both thrust magnitude and thrust node angles, for extreme values of both, horizontal trajectories (w.r.t. moon surface) with high thrust magnitudes are obtained. Higher thrust magnitude and more horizontal trajectories are both elements that increase total acceleration (for vertical trajectories the thrust force is in opposite direction of the gravity force so they cancel out more). The full MC shows no significant influence of the first four thrust angles on objectives/constraints, this is in agreement with one-at-a-time MC which shows some correlation in Fig. 9 but very weak influence on the objective space (see Fig. 5). Based on these results,  $\theta_5$  and thrust magnitude are suspected to have heavy interactions with all other variables while the rest of the decision variables have minor influence.

## 2.5 Linear Response Surface Analysis

The numerical results generated for the full Monte-Carlo analysis were used to fit a linear response surface including all possible (linear) interactions. Based on this method, the relative importance of each decision variable and its interactions can be quantified based on the normalised coefficients obtained through the regression analysis. Furthermore, this method can be used to explore the design space by providing a fitted function, which could be used (in ideal cases), for the optimisation itself. In this subsection, the fitted function considered has the form given by Eq. (5) (up to seven interactions), and the 128 coefficients were fitted using the Least Squares (LS) method (Eq. (6)), which minimises the sum of the squares of the residuals (Eq. (7)).

$$y = K_0 + \sum_i K_i x_i + \sum_{i \neq j} K_{i,j} x_i x_j + \sum_{i \neq j; i \neq k; j \neq k} K_{i,j,k} x_i x_j x_k + \dots \quad (5)$$

$$\hat{\beta} = (X^T X)^{-1} X^T y \quad (6) \quad r_i = y_i - \hat{y}_i = y_i - (X \hat{\beta})_i \quad (7)$$

In this formulation,  $x$ 's are the decision variables,  $K$ 's are the coefficients to be fitted,  $\hat{\beta}$  is the vector of the coefficients to be fitted,  $y$  is the vector of the objective values,  $X$  is the matrix of decision variables (# of rows is the number of simulations considered, # the number of terms to fit). The simulations which resulted in the violation of the constraints given in subsubsection 1.2.2 were not used to fit the function, to avoid interference from unfeasible propagations. The quality of the fit obtained will mainly be assessed using the degrees of freedom adjusted R-squared indicator ( $R_A^2$ ), which provides a measure of how well the fit explains the variations in the data (like  $R^2$ ), but is adjusted to account that adding coefficients will improve the  $R^2$  value without practically improving the fit<sup>8</sup>. The latter property is especially important as numerous coefficients are to be fitted. Additionally, the Root Mean Squared Error (RMSE), which is an estimate of the standard deviation of the data random component, is used as a direct measure of the error in the fit (note that it has the same units as the considered variable). The formulation of those indicators (using the Sum of Squared Errors, and the Sum of Squares about the mean) is given by,

$$SSE = \sum_i (y_i - \hat{y}_i) \quad SST = \sum_i (y_i - \bar{y}) \quad R_A^2 = 1 - \frac{SSE(n-1)}{SST(n-m)} \quad RMSE = \sqrt{\frac{SSE}{n-m}}$$

where  $\bar{y}$  is the average of the objective function considered (from the true data),  $n$  is the number of simulations used to fit the function, and  $m$  is the number of coefficients to fit. The method outlined above was applied for both the minimum corrective delta-V, and minimum propellant mass objective functions, yielding the indicators shown in Tab. 9. Note that the RMSE value for the fitted corrective delta-V surface response is on the high side (comparing to the associated  $R_A^2$ ), meaning that while the overall trend is well-captured, a relatively large error can be expected by considering the error single points. As a result, the response surface of for  $\Delta V_{corr}$  could be used in preliminary analysis to better understand the behaviour of the objective, but is not accurate enough to be used in an optimisation process directly. The fit for the propellant mass objective is neither accurate, nor captures the overall trends well enough to be used in preliminary design.

Table 9: Indicators of the quality of the fit to the data for each objective function.

Objective	$R_A^2$	RMSE
$\min \Delta V_{corr}$	0.921	105.5 m/s
$\min M_p$	0.687	119.6 kg

As an example, Fig. 24 provides a clear case of a parameter having a large influence on the objectives, but the overall trend being much better captured for the  $\Delta V$  objective (general upwards linear trend with a few overshoots for higher thrusts). The primary reason for this result is that the delta-V objective follows an overall linear trend with respect to decision variables and interactions, while the consumed propellant mass has a more non-linear behaviour. Following, the relative importance of the decision variables and their interactions was quantified by normalising Eq. (5), and making the variables non-dimensional. That is, each term was formulated as  $b_i x_i = \frac{b_i \tilde{x}_i}{\bar{y}} \tilde{x}_i = \tilde{b}_i \tilde{x}_i$ , which permits to compare the

<sup>8</sup>URL: <https://nl.mathworks.com/help/curvefit/evaluating-goodness-of-fit.html> [ONLINE, accessed on 12/06/2023].

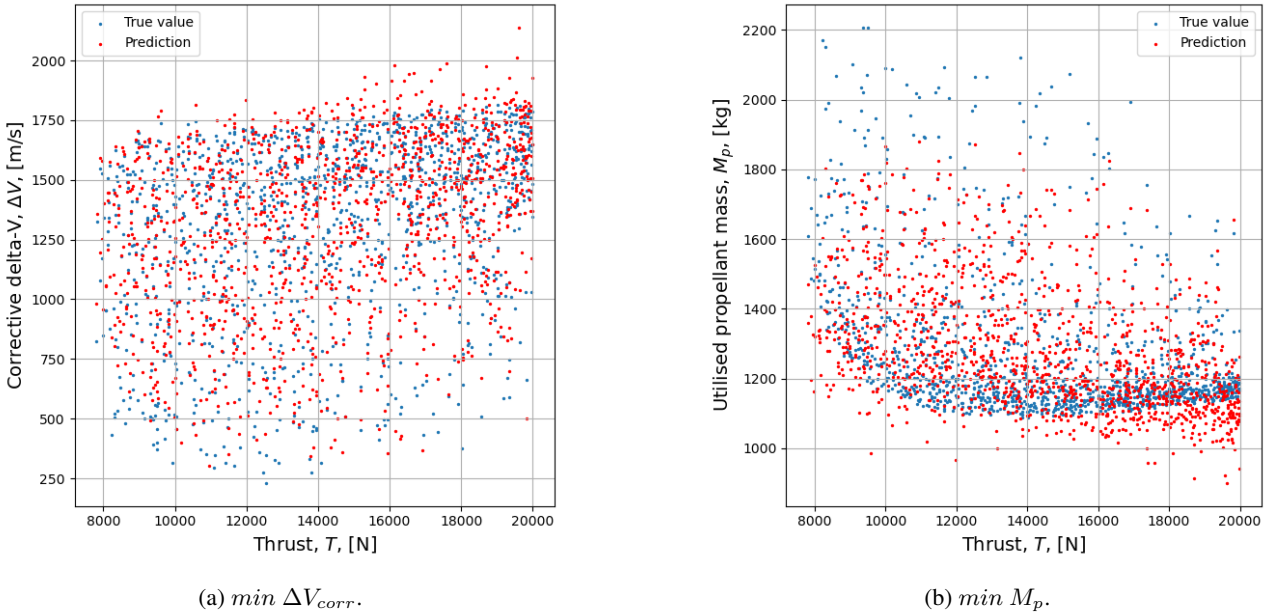
(a)  $\min \Delta V_{corr}$ .(b)  $\min M_p$ .

Figure 24: Comparison of the response surface predictions and the true propagations on the objective functions values. relative importance of each term in the fitted function using the  $\tilde{b}_i$ 's (which are related to a percentage contribution of the parameter to the objective value). The major components of the response surface for each objective function are shown in Tab. 10.

Table 10: Most important terms, and their relative magnitude, for the propellant mass and delta-V objectives. All parameters having a contribution larger than  $\sim 5\%$  are shown. Note that those relative importances may not be as accurate as given by other methods, due to the simplicity of the linear regression model.

Objective	Major components: $\tilde{b}_i$	
$\min \Delta V_{corr}$	Constant: 1.34 $\theta_5$ : -0.72 $T\Delta t\theta_5$ : 0.22 $\Delta t$ : -0.17	$T\theta_5$ : 0.14 $T\Delta t$ : 0.13 $T$ : 0.08 $\Delta t\theta_5$ : 0.05
$\min M_p$	Constant: 0.73 $\theta_5$ : 0.56 $\Delta t$ : 0.25	$T\theta_5$ : -0.25 $T\Delta t$ : -0.17 $\Delta t\theta_5$ : -0.17

From Tab. 10, a few conclusions can be drawn: (1) A constant term is the major component of both objectives, indicating that the value obtained is likely always in about the same range, and the parameters permit to tune the exact value. (2) For both objectives,  $\theta_5$  is the second most important component of the fit. This could be expected as that parameter determines greatly the orientation of the velocity vector while reaching the 100km altitude mark and on the time taken to reach it, having a large impact on both  $\Delta V_{corr}$  and  $M_p$ . Additionally, a larger  $\theta_5$  (up to  $90^\circ$ ) indicates a shallower trajectory, which is favourable for the delta-V, but leads to larger burn times and gravity losses (against  $M_p$  objective). (3) The thrust magnitude has a driving importance, but is mostly present through interactions with other decision variables. This can be expected as the thrust used in the propagation is a vectorial quantity applied over a certain time period, which is linked to  $\theta_i$ 's and  $\Delta t$ , as reflected above.

Compared to the lunar ascent itself, the corrective delta-V necessary to enter the design orbit was modelled through large simplifications (impulsive shot). This lack of details of the dynamical model could result in some trajectories deemed as feasible, while no practical manoeuvre would permit to enter the orbit (for large necessary corrective delta-V). This shows the importance of the minimisation of the necessary  $\Delta V_{corr}$  as a result of the model simplification. While this objective can be considered as the most important, the fit obtained is very good already, and improving the fit of the second objective (propellant mass) would be more useful for design purposes. Therefore, the latter will be considered into more details in this section and the next. For this objective function, Fig. 25 shows the error of the prediction compared to the value obtained from the propagations. It is clear that Figs. 25d, 25e, 25f, and 25g ( $\theta_1, \theta_2, \theta_3, \theta_4$ ) show no particular trend, meaning that the error is likely more dominant through other parameters. Fig. 25a shows a significant trend similar to a parabola centred on  $\sim 12$ kN, confirming that the thrust magnitude plays an important role in the trajectory, but that a linear fit is inappropriate. This is expected as a larger thrust means a shorter trajectory and less gravity losses, meaning that less fuel is used, until a levelling-off where the gravity losses become negligible (this trend cannot be represented by a linear profile; Fig. 7). Furthermore, another strong trend is found in the error of the response surface as a function of  $\theta_5$ . The error is small and contained between  $\pm 150$ kg for negative values, but explodes past  $\theta_5 = 0$ . This can be explained from

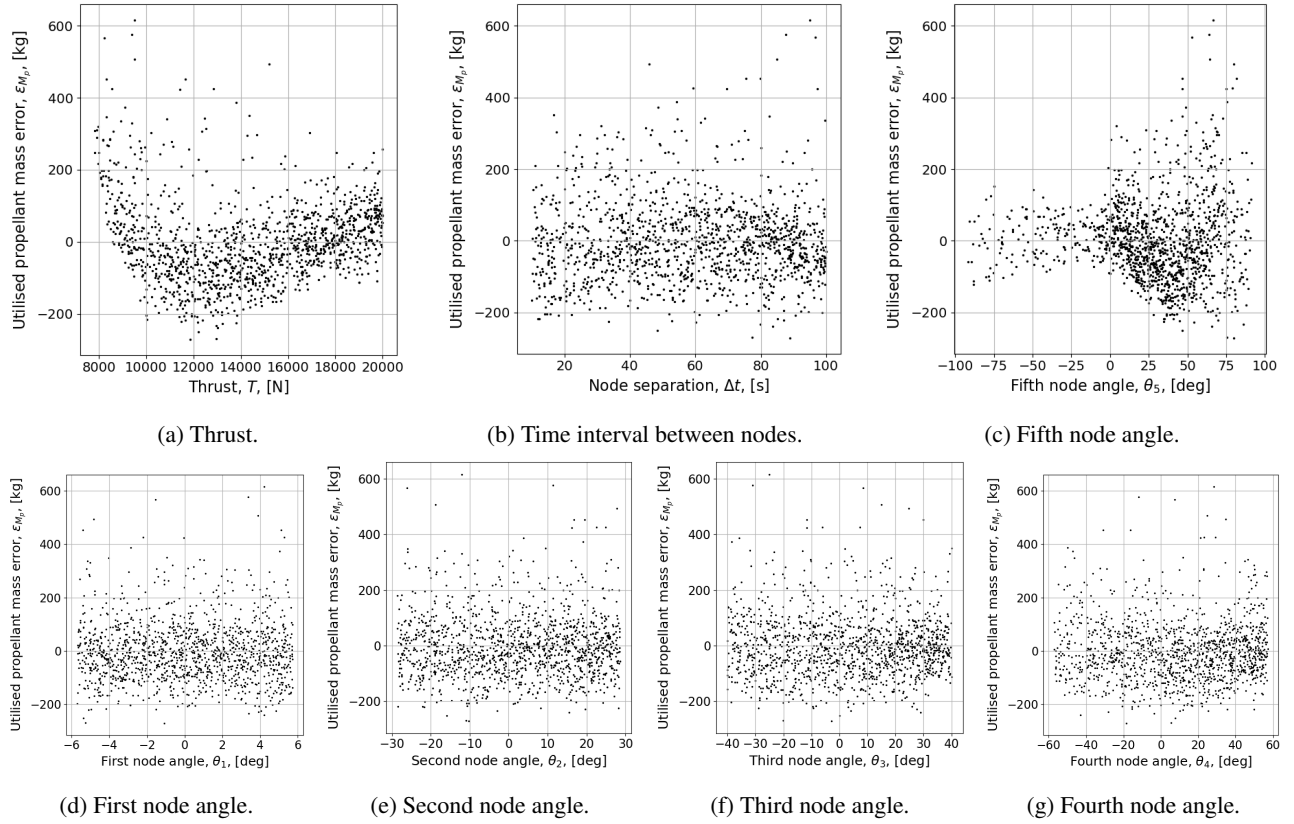


Figure 25: Error between the prediction of the response surface and the associated propagation data.

Fig. 19, where the behaviour is mostly constant for  $\theta_5 < 0$  but parabolic for  $\theta_5 > 0$  (due to the propagations violating the constraints being excluded from the analysis).

## 2.6 Extended Response Surface Analysis

The linear response surface for the propellant mass objective was improved through the addition of non-linear contributions. First, the result from the previous section was simplified to only include terms with  $|\tilde{b}_i| \geq 1.1\%$ . As a result, the fit  $R_A^2$  decreased to 0.66 and the RMSE increased to 125 kg, but this allows for a clearer picture of the function being adjusted (10 coefficients instead of 128). Then, the following modifications to the base functions were made:

- The terms containing the node angles values ( $\theta_i$ 's) was replaced by two terms:  $\cos(\theta_i)$  and  $\sin(\theta_i)$ . Angles generally appear through trigonometric functions in physics, and having both cosine and sine permits to obtain phase shifts (by assigning different weights to those terms). After this change,  $R_A^2 = 0.72$  and  $RMSE = 113.4\text{kg}$ .
- Following, considering Fig. 7, it seems like the thrust magnitude has a shape similar to a  $1/x$  profile. Therefore, the contribution of thrust in the interactions was replaced by  $1/T$  when it is combined with an angle (eg.  $T\theta_5$  became  $\frac{\cos(\theta_5)}{T}$  and  $\frac{\sin(\theta_5)}{T}$ ). However, the interaction with the time between each node was found to yield better result in the form  $T\Delta t$  and therefore remained unchanged. The physical reason behind this is unknown, but it could be argued that this term represents a direct mass contribution:  $\Delta M_p = \frac{T}{I_{sp}g_0}\Delta t$ . Furthermore, the thrust linear term was replaced by  $(\frac{1}{T})^2$  due to the shape of Fig. 7 and the parabolic nature of the residuals. As a result,  $R_A^2 = 0.88$  and  $RMSE = 73.8\text{kg}$ .
- At last, it can be seen from Fig. 11 that the fuel mass objective behaves roughly parabolically with the fifth node angle value. Therefore, the term  $\sin(\theta_5)^2$  was added to the base function. This results in  $R_A^2 = 0.89$  and  $RMSE = 72.2\text{kg}$ .

Overall, the use of  $1/T$  instead of  $T$  in the interactions and the addition of  $1/T^2$  to the basis functions resulted in the largest increase in fitting quality of the data. The final fitted function has the form,

$$\begin{aligned}
 M_p = & 2460 - 347\cos(\theta_5) - 90.4\sin(\theta_5) - 11.1\Delta t + 1.97 \cdot 10^6 \frac{\sin(\theta_5)}{T} - 2.32 \cdot 10^7 \frac{\cos(\theta_5)}{T} - 1.36 \cdot 10^{-4} T \Delta t \quad (8) \\
 & - 0.894\sin(\theta_5)\Delta t + 16.7\cos(\theta_5)\Delta t + 7.30 \cdot 10^4 \frac{\sin(\theta_4)}{T} - 2.17 \cdot 10^6 \frac{\cos(\theta_4)}{T} - 6.99 \cdot 10^4 \frac{\cos(\theta_2)}{T} \\
 & - 4.11 \cdot 10^6 \frac{\sin(\theta_2)}{T} - 3.68 \cdot 10^4 \frac{\Delta t \cos(\theta_3) \cos(\theta_5)}{T} - 909.1 \frac{\Delta t \sin(\theta_3) \sin(\theta_5)}{T} + 1.90 \cdot 10^{11} \frac{1}{T^2} \\
 & - 296\sin(\theta_5)^2
 \end{aligned}$$

Which results in  $R_A^2 = 0.886$  and  $RMSE = 72.2\text{kg}$  (previously:  $R_A^2 = 0.687$  and  $RMSE = 119.6\text{kg}$ ), providing a much better fit than the previous linear fitted function. The residuals are shown in Fig. 26, showing that the trend

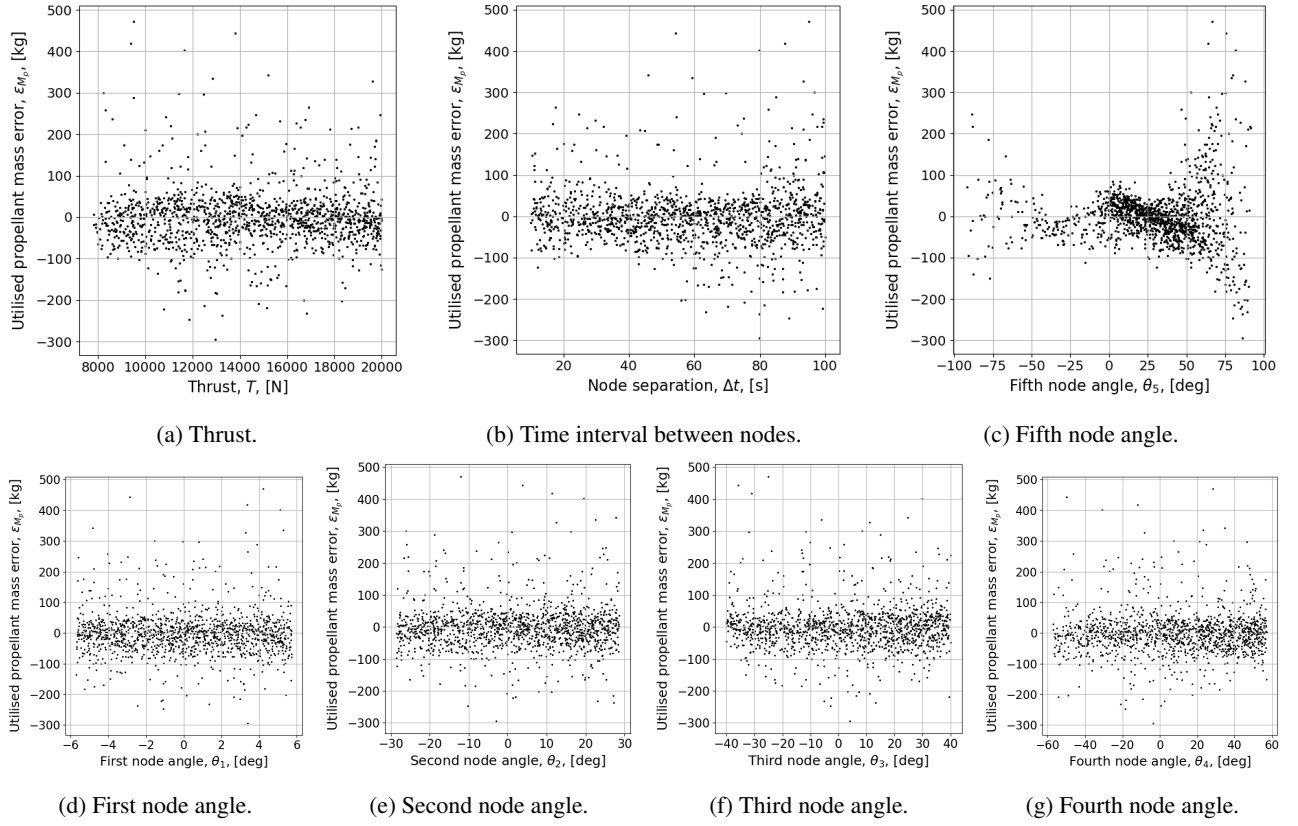


Figure 26: Error between the prediction of the non-linear response surface and the associated propagation data.

was mostly removed for the thrust dependence, but a trend resembling a third order polynomial persists. No better basis function was found to remove this trend, but aiming to implement higher order polynomials could help to resolve this issue. While this fit performs well, a better result was expected for the residuals as a function of  $\theta_5$ . This fit could be used to better understand the trends of the objective function and provide guidelines in the optimisation process, but is not accurate enough to be used in the optimisation process directly.

## 2.7 Full Factorial Design

In this section, a two-level full factorial design was done to study the importance of each decision variable as well as the importance of combinations of decision variables. Using this, and the other analysis methods discussed in this chapter, to best set up the problem for the optimization to come.

For the Factorial design, it was asked to keep the decision variable ranges to the same as those performed in previous sections. However, since these ranges have been set quite wide, to those in Tab. 11, most propagations failed to meet the requirements and are not representative. As a matter of fact only 16 out of 128 propagations were valid (equalling 12.5 %), which is insufficient to draw proper conclusions on the importance of each parameter.

As the minimum value of, for example, the thrust has been set to be sufficient to just achieve liftoff, and also very extreme node angles are taken, it makes sense this low thrust will not be sufficient to reach orbit. For this reason, it has been decided to vary the ranges by a fixed fraction around the previously used nominal values.

Table 11: Original decision variable range

	Thrust [N]	Node spacing [s]	N 1 [rad]	N 2 [rad]	N 3 [rad]	N 4 [rad]	N 5 [rad]
<b>Nominal values</b>	10.0E3	80	0.05	0.25	0.35	0.5	0.65
<b>Lower limit</b>	5.0E3	10.0	-0.1	-0.5	-0.7	-1.0	-1.3
<b>Upper limit</b>	20.0E3	100.0	0.1	0.5	0.7	1.0	1.3

Using this method also comes with another challenge, namely selecting the nominal value and ranges of which is varied. Using a to-be-explained ANOVA method the relative importance of each primary decision variable was determined for both a range of nominal values (in this case of the first decision variable: thrust) and a range of fractions for the decision variable range. The results of this can be found in Fig. 27, where the bar represents the average of all tested values, and the vertical bar is the range within each individual outcome. In this case, the range was varied from 5% to 20% and the thrust from 8,000 N to 14,000 N. Where it can clearly be seen that varying the thrust has a considerably larger effect than the variable range.

Despite these considerations, it is still decided to use the nominal values (as described in Tab. 11 as used in both Monte-Carlo analyses, to keep the comparison more similar. Selecting proper nominal variables for each decision variable would

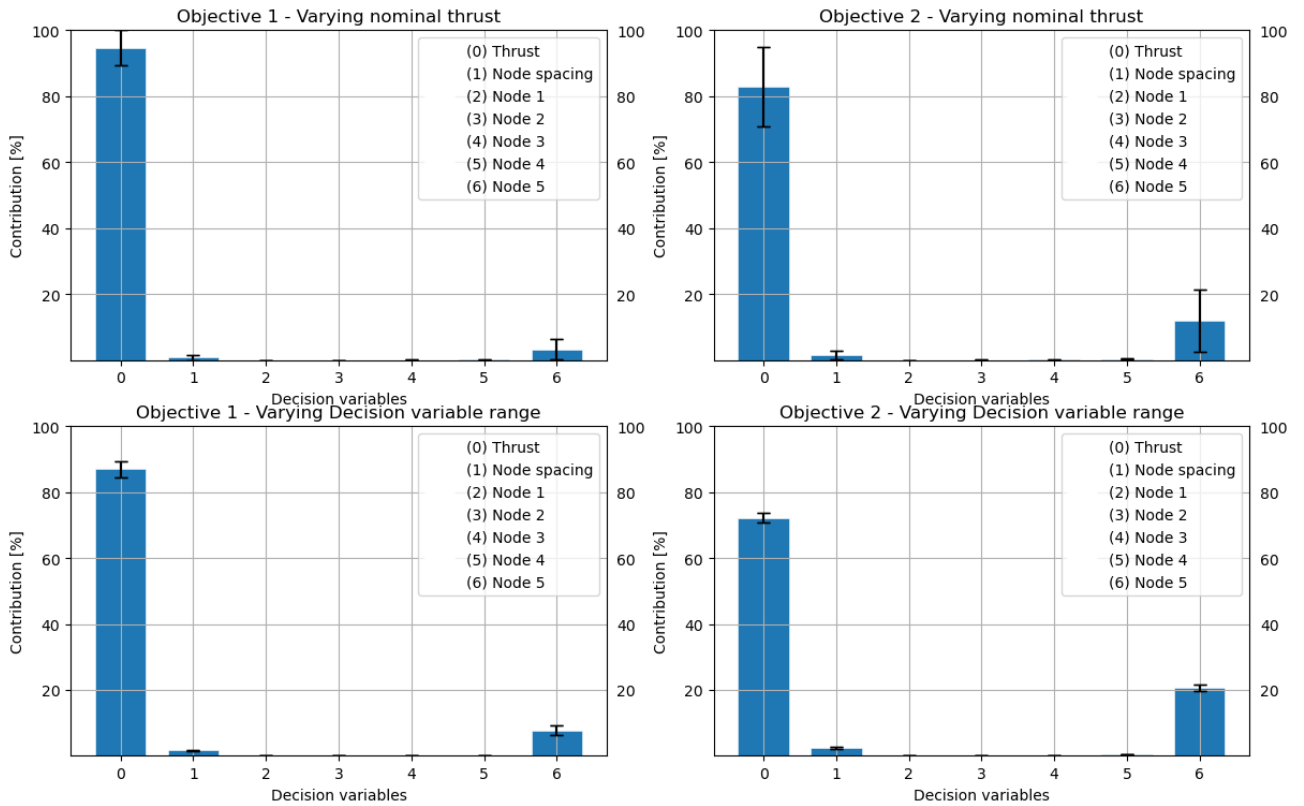


Figure 27: Contribution uncertainty for varying thrust magnitude and parameter variation range.

become an optimization process on its own, especially when considering cross-related effects. This would go beyond the purpose of performing the Factorial Design analysis and it was therefore left out. It is however decided to still use the varying range as implementation is quite easily done and it provides additional insight into the importance of each parameter over a different range. To remain within the original decision variable range a maximum variance of 25% is chosen, going any higher would set the maximum node spacing to be larger than 100 s compared to the 80 s nominal case.

Using the established ranges the two-level full factorial design can be performed, which is essentially a parameter variation over all decision variables. One by one each decision variable is tested for both the minimum and maximum case (two levels) and the fitness is determined. Using 7 decision variables over two levels results in  $2^7$  or 128 different combinations.

These results will then be analyzed using the analysis of variance (ANOVA) method. Which is essentially a method to determine the impact of changing one variable by comparing the difference from the average results when this variable is high and when it is low. This is done using the sum of squares ( $S_i$ ), calculating the sum of results for decision variable  $x_i$  at each level k (-1,+1). The total of sum of squares is then divided by the number of levels ( $N_L$ ) and the number of experiments at each level ( $N_k$ ), in this case 2 and 64 respectively. This results in Eq. (9) and can be used for each decision variable.

$$S_i = \frac{1}{N_L} \frac{(\sum^n y(x_i^+) - \sum^n y(x_i^-))^2}{n_k} \quad (9)$$

The relative importance is then calculated by finding the fraction of sum of squares for this decision variable of that of the total ( $S_T$ ), as done in Eq. (10).

$$P_i = \frac{S_i}{S_T} * 100\% \quad (10)$$

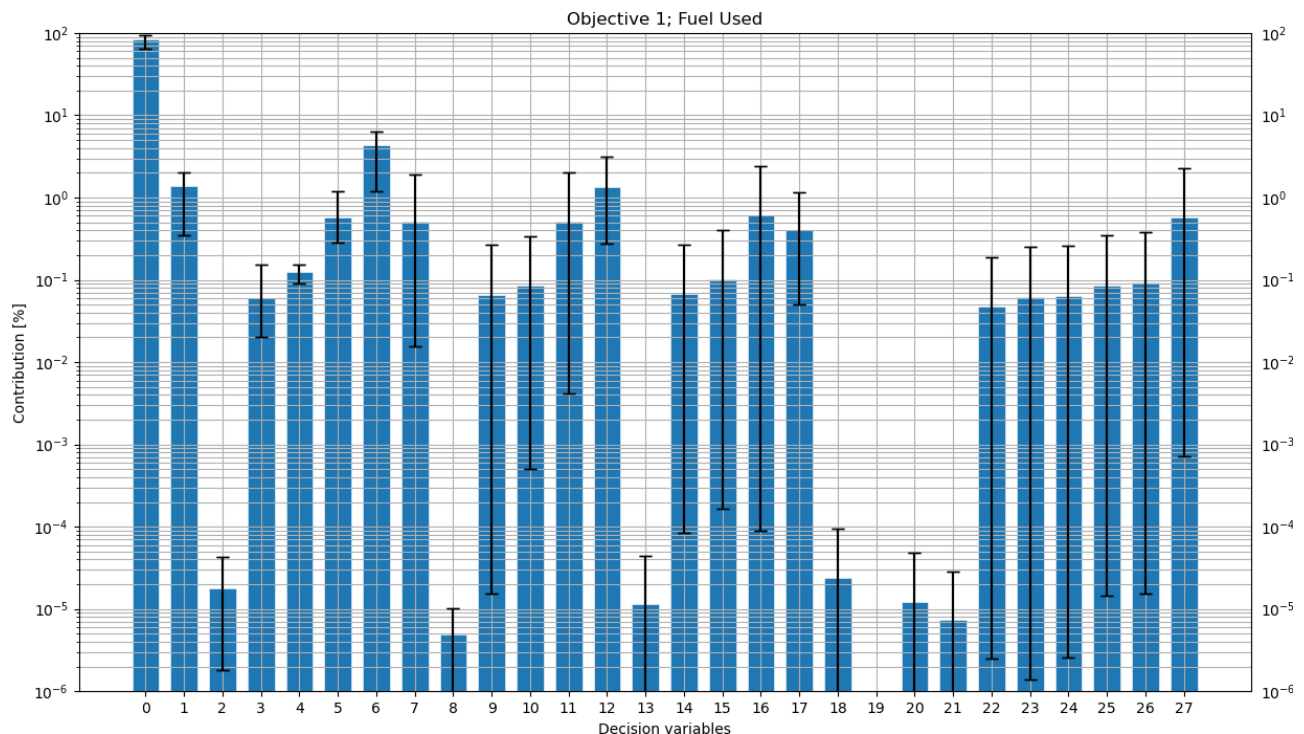
The total sum of squares can be calculated by finding the sum of deviations from the average, or by calculating the sum of results and subtracting the correction factor CF. Which is essentially the sum of results squared over the number of results, as shown in Eq. 11.

$$S_T = \sum_{i=1}^N (y_i - \bar{y})^2 = \sum_{i=1}^N y_i - \frac{T^2}{N} = \sum_{i=1}^N y_i - CF \quad (11)$$

Using this analysis method the relative importance for each variable is determined, as seen in Fig. 28. Note that not only each decision variable has been considered but also the correlation between each of the decision variables. In this case if both decision variables are at either a minimum or maximum the effect is high (+1) and if one is minimum and one maximum the effect is low (-1). These values are then used to fill the Yates array to a 28x128 array.

First, solely looking at the decision variables themselves and neglecting the cross-correlations it can immediately be seen that thrust is the predominant variable for this optimization problem. Over both objectives, it has a relevance of 80% over all combinations. With an average of 2.55 % the nodal spacing also has not much significance over the variables, however it indirectly affects the importance of the nodes. Currently, the nominal spacing is set to 80 s, which is quite high within the variable range. If the nodes were to be closer together, the nodes were to gain more relative importance over the thrust. The nodes themselves show a clear increase in importance for each nodal index, for both objectives. This is likely due to initial nodes being fairly straight up and not that influential towards the final trajectory, whereas later on the vehicle rotates and the nodes become slightly more important. The last node has a significantly higher importance, simply due to the vehicle flying longer under this angle. Each node is spaced 80 s apart, whereas the last node angle is used for the remaining part of the flight, which is always larger. From these results it can thus be concluded that the thrust, node spacing, and last node have a driving importance in this optimization problem.

Now looking at the cross-correlations as well, results behave quite as expected. For both the correlations revolving around the thrust variable and the node spacing variable, the correlations are scaled but still distributed very similarly to their uncorrelated importance. For the nodal correlations results start to behave a little strange, as it would be expected that the correlation importance lowers as the nodes are farther apart. Which is still the case for the Node 1 correlations. However, for node 3 (and in the case of the second objective node 4), increasing correlations can be seen as the node index increases. It could be argued that the increasing uncorrelated importance of the later nodes causes this, but the correlation between nodes 1 and 5 is the lowest of all, in spite of the high importance of solely node 5. Since the nodal cross-correlations are very low compared to all the others no additional research is done on this unexpected behaviour, as it is unlikely to impact further work.



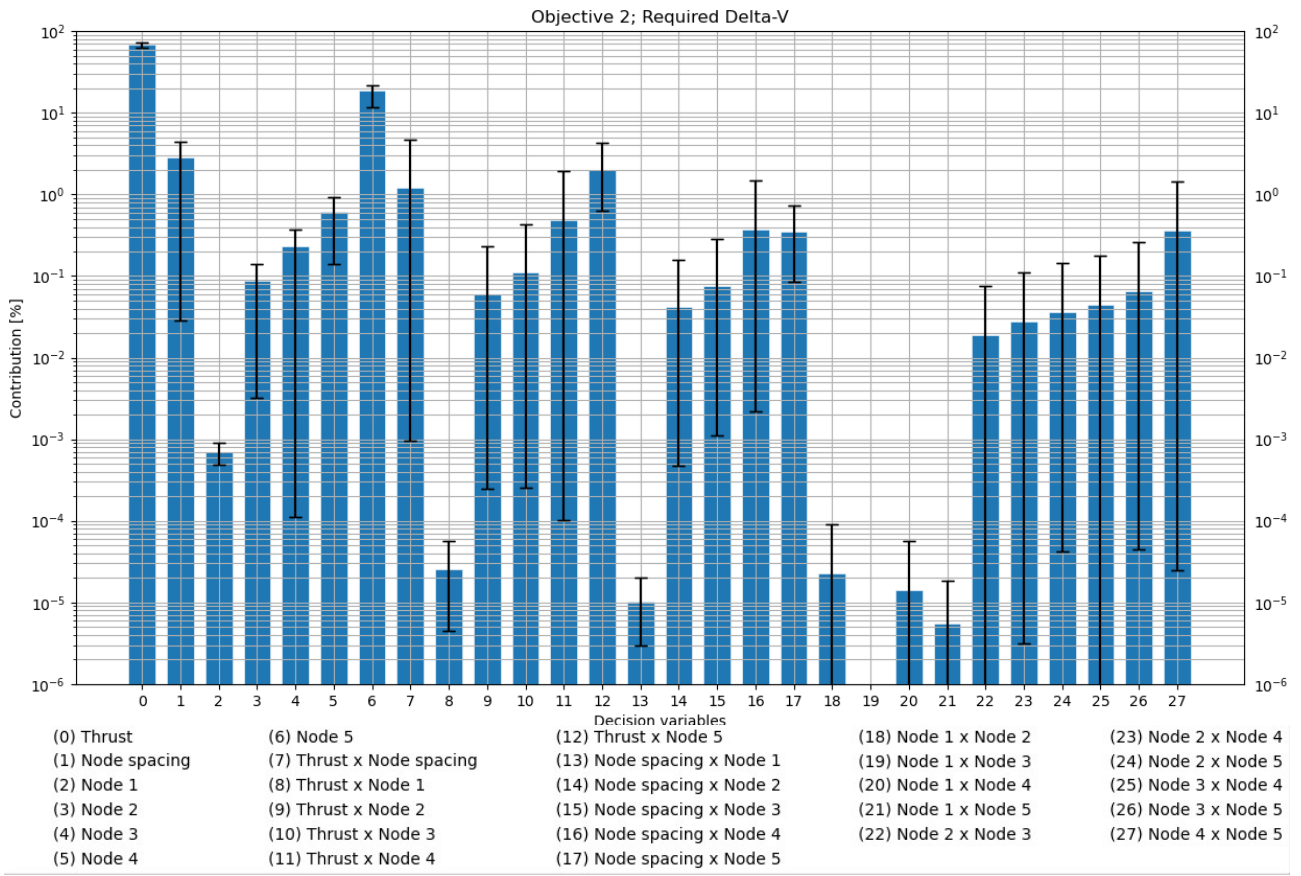


Figure 28: Decision variable contribution for the Delta V objective

### 3 Reflection on Optimisation Problem Formulation

In this section, the design space exploration as well as the underlying optimization problem will be analyzed based on the work performed in Section 2. Using this analysis a final design space and optimization problem will be selected to be performed in later stages of the design.

#### 3.1 Design Space Exploration Analysis

In the previous section, a total of three design space explorations have been performed; both one-at-a-time and full Monte-Carlo as well as factorial design. After this, the full Monte-Carlo results were fitted using linear and extended response surfaces. Each method carries its own strengths and weaknesses.

The one-at-a-time MC analysis is easy to interpret, fast to implement, and is able to show the isolated effects of varying each decision variable independently, yet it is incapable of showing dependencies between different variables. In Subsection 2.2 the results of one-at-a-time MC provide insight into the linear behaviour of node spacing, discontinuities in thrust magnitude and  $\theta_5$  and quadratic behaviour of the first four thrust angles to both objectives. The disadvantage of varying parameters independently is that only a limited part of the design space is covered. Furthermore, the behaviour of the constraint functions is not readily obtained using one-at-a-time MC since all non-varying decision variables are kept at their nominal value, thus a lot of violated or previously impossible runs are not shown. Combined with inherent biases by perhaps ill-defined nominal parameters, ranges, and Sobol distributions, the one-at-a-time method is subject to the risk of making false conclusions on the overall design space.

This limited-design space exploration problem of the one at a time method, is better handled by the full Monte-Carlo analysis, which does show the full design space with all correlations, but it is harder to draw conclusions due to the amount of interactions. The results for  $\theta_5$  in full MC better captured the physical problem of lunar ascent since in combination with all other variables only the trajectories launching east are feasible, unlike the one-at-a-time MC analysis where this correlation was not observed, see Figs. 14 and 15). In order to analyse the data provided by the full MC simulation, linear and non-linear response surfaces can be produced. The former is straightforward to implement and directly shows results on which parameters are driving the objective functions the most, and may already produce a good description of the data. A non-linear response surface can be used to expand on the linear model produced and reduce the residuals between the data and the prediction from the fitted function, but it can be very time-consuming and challenging to determine which basis functions should be used. The response surfaces (linear for the corrective delta-V objective and non-linear for the propellant mass objective) produced in this work could be used to find areas of interest in the design space, where the optimisation process can take place.

Factorial design provides a more systematic approach to the design space problem than Monte-Carlo and is capable of directly showing the importance of each decision variable and its influence. Mostly consistent conclusions with factorial

and one-at-a-time MC are obtained about thrust magnitude and  $\theta_5$  as dominant parameters. This setup however makes it difficult to get it right, as briefly discussed in Subsection 2.7 results depend strongly on the decision variable range, and getting this right can become somewhat of an optimization itself. With a high amount of decision variables this method is not feasible due to the exponentially increasing amount of runs. Valuable information into parameter correlations are shown, but there is no visual insight into the design space like in MC.

### 3.2 Optimization Problem Trends

The results of all three design space exploration methods show a number of correlations as well as some discrepancies. One thing the one at a time MC and factorial design agree upon is the increasing importance of each thrust angle node. Where it is always more influential for the delta-V objective than the fuel mass objective. This makes sense as a trajectory going straight up will be terminated by the maximum altitude constraint and will not use that much more than a curved flight path, however when looking at the delta-V required to adjust the final orbit this difference is much larger. For the full MC analysis it is very difficult to say anything useful about the influence of the first 4 nodes as for the whole range of generated values, all ranges in the objective space can still be reached. On top of this all models agree that the node spacing also is of significance, albeit much less than that of the fifth node angle.

Where conclusions start to deviate is at the importance of the thrust. As per the linear response surface performed on the full Monte-Carlo, it does carry some significance but not as much as the nodes and node spacing. Whilst for the one-at-a-time Monte Carlo the objective performance varies strongly with the thrust magnitude. The same goes for the factorial design where the importance is estimated to be up to 80% of the total. Looking at Figs. 7 and 8 it can be seen that the nominal parameter value of 10,000 N used in the factorial design is in a highly nonlinear regime of the thrust range. This may cause it to falsely show high importance in the parameter design, whereas a higher nominal thrust would not have.

As for the cross-correlations between the decision variables both the linear response surface and factorial design agree upon the three most significant combinations:  $T \times \Delta t$ ,  $T \times \theta_5$ , and  $\Delta t \times \theta_5$ . However, the absolute value of importance is much higher for the response surface than that of the factorial design and ANOVA. As one-at-a-time Monte-Carlo only considers one variable in each case it cannot detect cross-correlations and therefore cannot be compared.

Regarding the design space constraints, some of them are more dominant in causing failed propagations than others. In the lower thrust regime, it is mostly the minimum altitude that is the limiting factor, as low thrust in combination with high thrust angles is most often not sufficient to reach orbit and the ascent module crashes down to the Lunar surface. For high thrust and low node angles, the trajectory is fairly straight, and the limiting factor most often becomes the delta-V buffer, as it requires a large manoeuvre to get to the right orbit. Constraints like the maximum rotation rate and maximum acceleration are rarely limiting as seen by Figs. 17 and 16 respectively. Lastly, there is the fuel mass constraint, which is also a limiting factor in some cases like the high node angles in Fig. 14. Any other constraint mentioned in Tab. 4 is inherently dealt with by the propagation setup. Worth mentioning is that the maximum altitude constraint, which is set at 100 km, does constrain the solutions to trajectories that do not overshoot the target orbit first after which they reach the target orbit. If such an optimum trajectory would exist it cannot be found with the current constraints.

The last trend that can be found in the results is the competitiveness of the two objectives set from the optimization problem. Fig. 19 shows this through the increasing gradient, signalling lower delta-V needed, for increasing fuel mass. Meaning that both objectives sufficiently compete and are still considered fascinating focus points for this optimization problem.

### 3.3 Final Design Space and Optimization Problem

The exploration of the design space has led to a number of changes in the constraints, decision variables, and objectives. For the constraints, it became evident that a number of them are redundant. Previously the minimum thrust defined in the decision variables was set at 5 kN, which was below the constraint on minimum thrust. This part of the design space is a waste and so the decision variable Thrust was given a new minimum of 7.61 kN, equal to the lift-off weight. This makes the minimum initial thrust load constraint redundant. Given the same thrust range the maximum time constraint and maximum acceleration will too be redundant. The maximum thrust of 20 kN at minimum thrust, equal to  $M_{dry}$ , is equal to  $8.89 \text{ m/s}^2$ . This is far below  $6g$ . Additionally, at the minimum thrust of 7.61 kN and the fixed ISP of 452 s, the mass flow is equal to 1.72 kg/s. Making the maximum propagation time 1426.3 s, and so the maximum time constraint irrelevant. Despite their redundancy, the requirements are all left in for completeness and show vehicle limitations. If thrust ranges or other variables were to change in future studies, like that of variable thrust design for the bonus question, these constraints may become relevant. All other constraints still are relevant and left the same, all can be found in Tab. 12

Ideally the delta-V buffer constraint would allow for some room to complete the docking procedures as well as safety margins, though as the objectives revolve around fuel mass used and delta-V needed, this variable is already optimized for and an additional constraint is not needed. If it were, however, the case that the optimal trajectory has only a small delta-V buffer after all manoeuvres the optimization may need to be revised. Additionally, if the calculated optimum were to have a final fuel mass of 400 kg (eg.), it would be best to reiterate on the problem and start the optimization with around 400 kg less fuel mass (or slightly less to keep some buffer). At this stage it is uncertain if the current assignment allows room for this type of optimization, but if possible it will be taken into account.

Table 12: Final constraints functions chosen for optimization.

Constraint	Description
$r_0 = r_M + h_0, \quad \lambda_0 = 23.4333^\circ, \quad \phi_0 = 0.6875^\circ$	Initial state
$\gamma_0 = 89^\circ, \quad v_0 = 10m/s, \quad \psi_0 = 90^\circ$	Initial state
$I_{sp} = 452s$	Specific impulse
$t_{max} \leq 3,600s$	Maximum time
$\psi_0 = \frac{T}{M_0 g_m} > 1$	Minimum initial thrust load
$a_{max} \leq 6g$	Maximum mechanical load
$h_{min} > 0km$	Minimum altitude
$h_{max} = 100km$	Propagation terminated using line-search at 100km
$M(t_e) \geq M_{dry} = 2250kg$	Minimum mass
$\dot{\theta}_{max} \leq 20deg/s$	Thrust angle rate constraint
$\Delta V_{buffer} = I_{sp} g_0 \ln\left(\frac{M(t_0)}{M(t_e)}\right) - \Delta V_{tar} \geq 0m/s$	Check if target orbit is reachable with remaining fuel mass

As for the decision variables, the change in minimum thrust has already been discussed. However, the thrust angle ranges have also undergone quite a large change. Firstly, it is fixed in Tab. 12 that the initial heading is 89 degrees, meaning it is slightly east. Propagating the trajectory westwards would always be inefficient as the initial eastward velocity would be counteracted, therefore the nodal ranges have been redefined to be only eastwards and all start at 0.0 rad. Additionally, looking at Figs. 9 and 10 it is hard to argue that the range of all nodes is sufficient to reach an optimum. Especially as both plots compare a different unit, fuel mass against delta-V. To gain more insight in the optimal ranges additional simulations have been run, where all thrust angles are varied from 0 to 90 degrees and plotted against total fuel consumed. This results in Fig. 29, where it immediately can be seen that some optimum lie outside of the currently used decision variable ranges in the design space. The design space is best used if the optimum is exactly in the middle, meaning all new thrust angle boundaries will vary between 0 and double the optimum, the final values are given in Tab. 13. The new boundary value of  $\theta_1$  being 0.8 rad will not lead to problems with the maximum angular rate constraint (20 deg/s). This is due to the lunar module requiring at least 10 s to reach the first thrust node located at 100m altitude and a final speed of 10m/s.

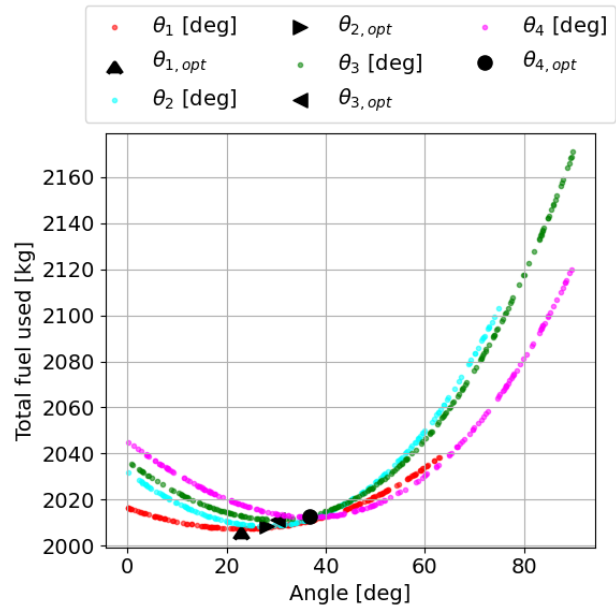


Figure 29: Total fuel mass used for different thrust node angles, using one-at-a-time Monte Carlo

Table 13: Final decision variables and ranges.

Decision variable	Definition and boundaries
Thrust magnitude	$7.61kN \leq T \leq 20kN$
Node spacing	$10s \leq \Delta t \leq 100s$
Thrust angle at node 1	$0.0rad \leq \theta_1 \leq 0.8rad$
Thrust angle at node 2	$0.0rad \leq \theta_2 \leq 1.0rad$
Thrust angle at node 3	$0.0rad \leq \theta_3 \leq 1.1rad$
Thrust angle at node 4	$0.0rad \leq \theta_4 \leq 1.3rad$
Thrust angle at node 5	$0.0rad \leq \theta_5 \leq 1.6rad$

The analysis in Section 2 has proven that both objectives are sufficiently competing and still in line with the aim of the optimization, for this reason, the objectives are kept the same. Note that in the future it will sometimes be opted to convert the delta-V objective to a manoeuvre fuel mass objective for more straightforward comparison to the fuel for ascent, like is done in Figure 29.

#### 4 Bonus Question - 3D Thrust Parameterisation and Time Variable Thrust Magnitude

To extend the optimization problem additional decision variables will be added to the analysis. Previously the thrust was defined to act along the YZ-plane in the vertical reference frame [10]. In addition to this a new angle ( $\psi$ ) has been introduced, acting in the XZ-plane. Both  $\theta$  and  $\psi$  act in the negative Z direction and positive X and Y direction. This has resulted in the thrust vector definition as described in Equation 12.

$$\vec{T} = \begin{bmatrix} \sin(\psi) \\ \sin(\theta) \\ -\cos(\theta) - \cos(\psi) \end{bmatrix} \quad (12)$$

In Figure 30 it can be seen that the  $\psi$  angle correctly influences the orbit. The line with no second angle implemented goes almost straight when looking in the XZ-plane, where the negative nodes make it move left and the positive ones move it to the right. To show the effect of changing the direction throughout the propagation a fourth line is plotted, showing that the ascent vehicle is now capable of manoeuvring right to left.

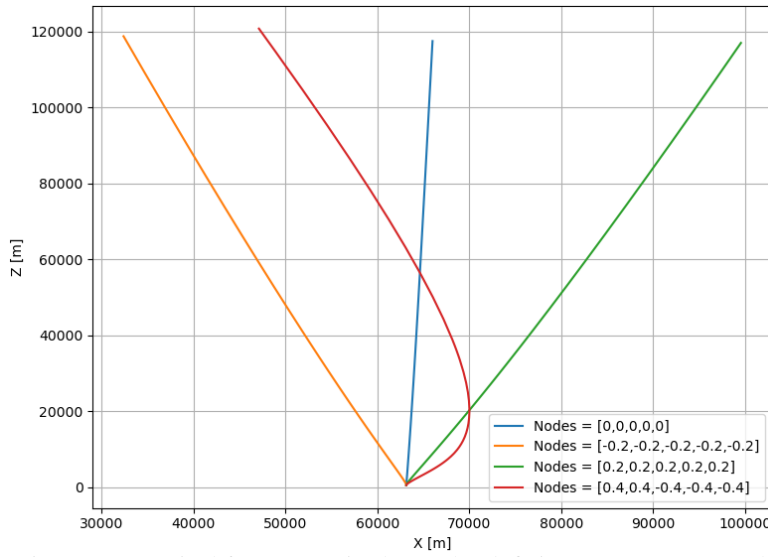


Figure 30: Vertical frame X-axis change by defining 3D vector control

To optimise the ascent phase better and make the problem more realistic, the thrust will be varied over the course of the propagation. The thrust magnitude will be redefined at each node, similar to the angles. To get a full thrust profile the Hermite-Spline interpolator is used to create a smooth thrust profile. These two changes have extended the decision variable list from the original seven up to 16, which now looks as follows:

- thrust parameters =  $[\Delta t, \theta_1, \theta_2, \theta_3, \theta_4, \theta_5, \psi_1, \psi_2, \psi_3, \psi_4, \psi_5, T_1, T_2, T_3, T_4, T_5]$

To assess the value of implementing this model extension a one-at-a-time Monte-Carlo analysis is performed using 400 runs, the same Sobol sampling as in Subsection 2.2, and the following nominal parameters [80.0, 0.05, 0.25, 0.35, 0.5, 0.65, 0, 0, 0, 0, 0, 10.0E3, 10.0E3, 10.0E3, 10.0E3, 10.0E3]. The thrust at each node is 10kN and the nominal  $\psi$  angles are all 0 deg so in the original thrust parameterisation plane. The same decision variable range is used as in Q1 with thrust now varying as in Q3c between 7.6 kN and 20 KN. Since the trajectory is supposed to reach a near equatorial orbit the additional angle  $\psi$  is varied at each node by  $\pm 0.1rad$ .

The objective spaces for varying the thrust magnitude at each node  $T_i$  and the additional angles  $\psi_i$  are presented in Figure 31 and Figure 32. It is observed that time variable thrust has a large effect on both objectives, while  $T_5$  seems to follow a trend different from the previous nodes suggesting that it has more influence on fuel mass consumed. The additional thrust angles  $\psi_i$  have almost no influence on the fuel mass consumed. This is also true for objective 2 except for  $\psi_5$ , which has a great effect on corrective  $\Delta V$  required, suggesting that modifying the trajectory after the last node to correct for the inclination and saves  $\Delta V$  later in the final inclination manoeuvre, part of objective 2.

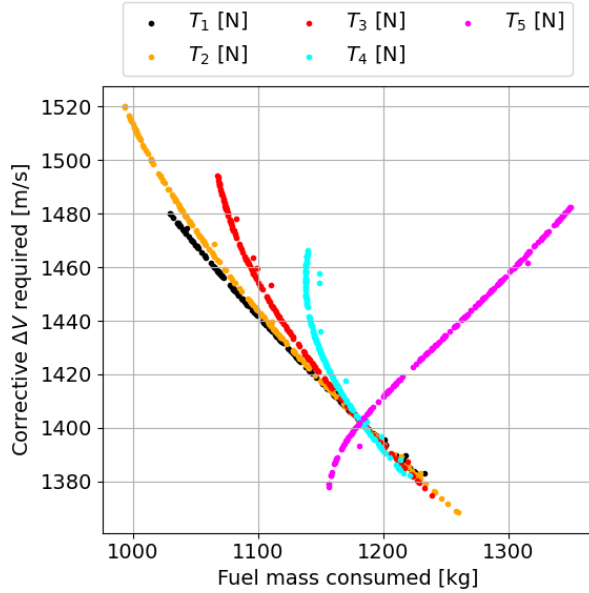


Figure 31: Objective space showing fuel mass consumed (kg) and corrective  $\Delta V$  required (m/s) for varying  $T_i$

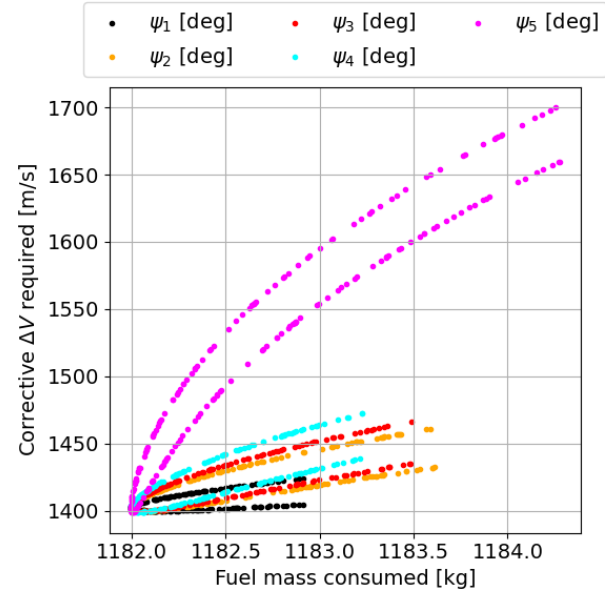


Figure 32: Objective space showing fuel mass consumed (kg) and corrective  $\Delta V$  required (m/s) for varying  $\psi_i$

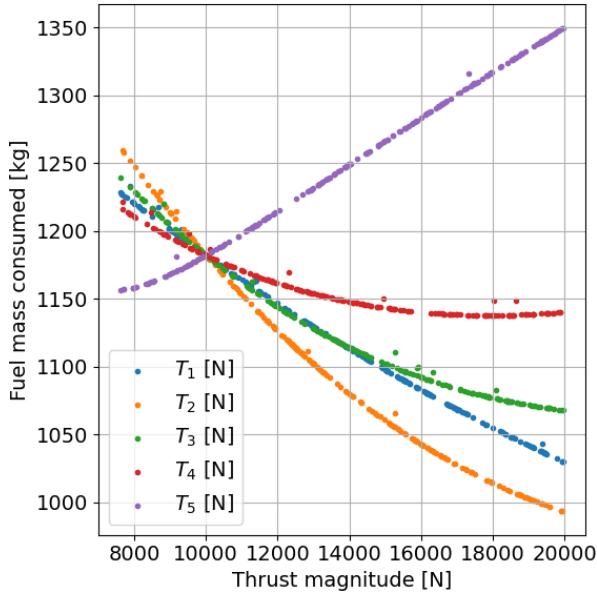


Figure 33: Fuel mass consumed (kg) for variation in thrust magnitude (N) at each node,  $T_i$ .

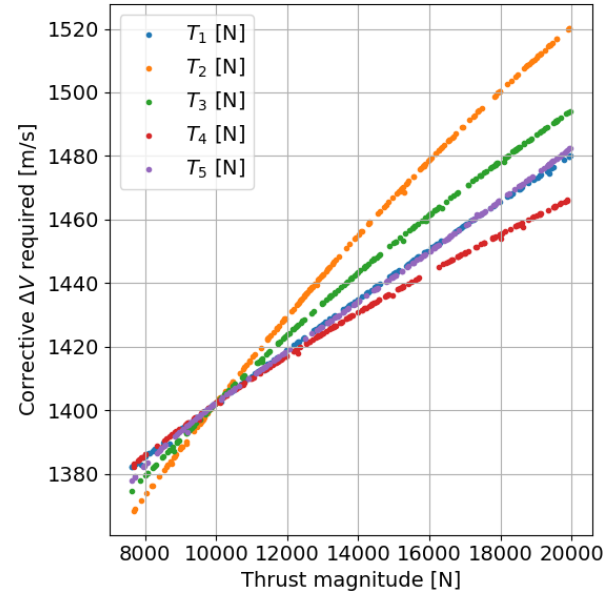


Figure 34: Corrective  $\Delta V$  required (m/s) for variation in thrust magnitude (N) at each node,  $T_i$ .

The influence of thrust magnitude on each objective is shown in Figure 33 and Figure 34. Increasing  $T_1$  to  $T_4$ , results in less fuel mass consumed as the trajectory is terminated earlier but objective 2 is minimised.  $T_5$  shows a different trend, leading to lower fuel mass consumed if lower thrust is used at the end of the trajectory which makes sense, as real rocket ascents tend to throttle down over time. The influence on objective 2 is similar for each magnitude. This analysis with independent variations in  $T_i$ , omits the possibility of defining a complete thrust profile, which can only be done in full Monte-Carlo but would be more optimal. In Figure 35 and Figure 36 it can be seen that changing the angles only slightly increases the fuel mass used, but has a significantly larger impact on the delta-V needed. This is in line with the results from Figure 32, where similar trends were discussed. As the thrust profile and termination conditions still rely on the YZ-plane, the actual trajectory does not become that much longer by adding an XZ-plane angle, which means not much additional fuel is needed. This angle change however does cause a larger discrepancy between the desired and reached orbit, which means the larger  $\psi$  the larger the correcting burn will need to be.

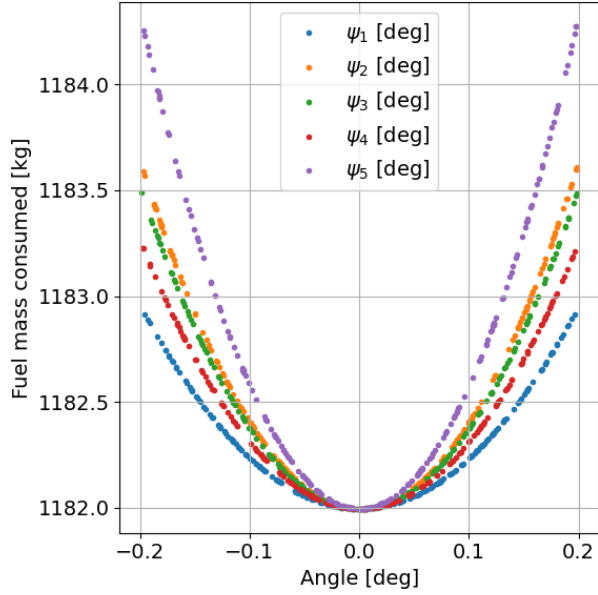


Figure 35: Fuel mass consumed (kg) for variation in  $\psi_i$  (deg).

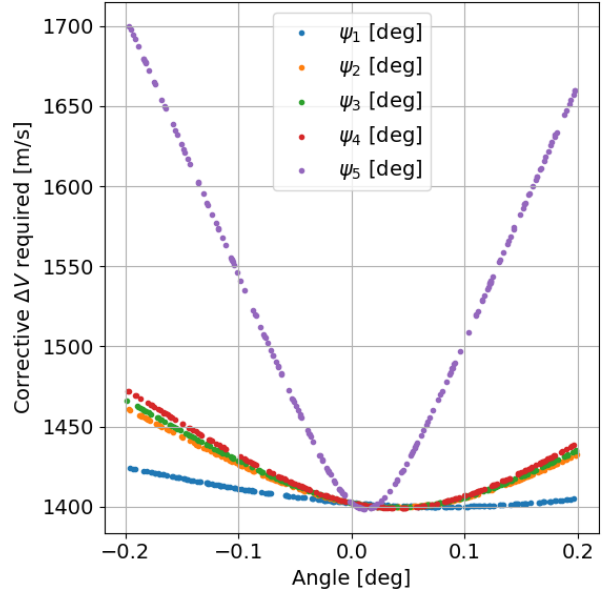


Figure 36: Corrective  $\Delta V$  required (m/s) for variation in  $\psi_i$  (deg).

The design space of the thrust vectoring shows there is for sure potential to improve the trajectory even further than the design space discussed throughout this assignment. Implementation would therefore be recommended for further analysis. Changing the thrust vector over three dimensions appears to increase the quality of the ascent problem slightly. Results in Figure 36 reveal that the optimal angle is slightly right of 0 rad, meaning that with some three-dimensional vectoring, the ascent profile can counteract perturbations encountered in the problem to require less  $\Delta V$  correction in the end. For this reason, it is recommended to implement both adaptions. This would mean an increase of 9 decision variables, making optimization a much more time-consuming process than before. There is a tradeoff between the time saved on not doing these additional computations and the slightly improved accuracy reached by those modifications.



## 5 Breakdown of contributions

Table 14: Breakdown of contributions of team members.

Section	Implementing (coding and post-processing)	Analysing (Discussion, thinking, etc.)	Reporting	Hours spent
<b>1.1 Problem Definition</b>	Implementation of the initial setup of the code : L. Veithen	All team members	L. Veithen	8
<b>1.2 Preliminary Optimisation Problem Formulation</b>	N.A.	D. Calliess and J. Voskuilen	D. Calliess and J. Voskuilen	J. Voskuilen : 3, D. Calliess: 7
<b>1.3 Verification of Numerical Accuracy and Objective and Constraint values</b>	M. van Doorn first did all coding work for the question. Then L. Veithen re-iterated on the verification of the numerical accuracy and added the benchmark analysis. The plot of the Range vs. Altitude remained M. van Doorn's work.	M. van Doorn & L. Veithen	The final reporting part of the numerical accuracy is L. Veithen's work. The part on the objective and constraint values is M. van Doorn's work.	M. van Doorn: 8, L.Veithen: 2
<b>2 Design Space Exploration - general contributions</b>	D. Calliess coded the fitness function, which could then be used for simulations.	This function was iterated upon a few times through discussions between D. Calliess and L. Veithen	N/A	D.Calliess 8h
<b>2.1 Sobol Distribution</b>	M. van Doorn	M. van Doorn	M. van Doorn	4
<b>2.2 One at a Time Monte-Carlo</b>	D. Calliess	D. Calliess	D. Calliess	15
<b>2.3 Full Monte-Carlo</b>	M. van Doorn	M. van Doorn	M. van Doorn	25
<b>2.4 Monte Carlo Methods Comparison</b>	-	D. Calliess & M. van Doorn	D. Calliess & M. van Doorn.	Each member: 3
<b>2.5 Linear Response Surface Analysis</b>	L. Veithen	L. Veithen	L. Veithen	22
<b>2.6 Extended Response Surface Analysis</b>	L. Veithen	L. Veithen	L. Veithen	8
<b>2.7 Full Factorial Design</b>	J. Voskuilen	J. Voskuilen	J. Voskuilen	J. Voskuilen : 20
<b>3.1 Design Space Exploration Analysis</b>	N.A.	J. Voskuilen & D. Calliess	J. Voskuilen & D. Calliess	J. Voskuilen : 3, D. Calliess 3
<b>3.2 Optimization Problem Trends</b>	N.A.	J. Voskuilen & M. van Doorn	J. Voskuilen & M. van Doorn	J. Voskuilen : 3, M. van Doorn: 2
<b>3.3 Final Design Space and Optimization Problem</b>	D. Calliess & J. Voskuilen	D. Calliess & J. Voskuilen	D. Calliess & J. Voskuilen	J. Voskuilen : 14, D. Calliess: 4
<b>Bonus question</b>	D. Calliess & J. Voskuilen	D. Calliess & J. Voskuilen	D. Calliess & J. Voskuilen	J. Voskuilen: 10, & D. Calliess: 10

# References

---

- [ 1] L. Veithen, “Propagation and optimisation - assignment 1,” Delft University of Technology, Tech. Rep., 2023.
- [ 2] K. F. Wakker, “Fundamentals of astrodynamics,” 2015.
- [ 3] D. Calliess, “Propagation and optimisation - assignment 1,” Delft University of Technology, Tech. Rep., 2023.
- [ 4] M. van Doorn, “Propagation and optimisation - assignment 1,” Delft University of Technology, Tech. Rep., 2023.
- [ 5] J. Voskuilen, “Propagation and optimisation - assignment 1,” Delft University of Technology, Tech. Rep., 2023.
- [ 6] J. Voskuilen, “Propagation and optimisation - assignment 2,” Delft University of Technology, Tech. Rep., 2023.
- [ 7] L. Veithen, “Propagation and optimisation - assignment 2,” Delft University of Technology, Tech. Rep., 2023.
- [ 8] D. Calliess, “Propagation and optimisation - assignment 2,” Delft University of Technology, Tech. Rep., 2023.
- [ 9] M. van Doorn, “Propagation and optimisation - assignment 2,” Delft University of Technology, Tech. Rep., 2023.
- [ 10] E. Mooij, “The motion of a vehicle in a planetary atmosphere,” *Delft University of Technology, Faculty of Aerospace Engineering, Report LR-768*, 1994.
- [ 11] G. P. Sutton, *Rocket Propulsion Elements*, 7th ed. John Wiley & Sons, 2001.
- [ 12] M. Interbartolo. “Apollo lunar module propulsion system.” (2009), [Online]. Available: <https://ntrs.nasa.gov/api/citations/20090016298/downloads/20090016298.pdf> (visited on 06/06/2023).